

Video-driven Neural Physically-based Facial Asset for Production

LONGWEN ZHANG*, ShanghaiTech University, China and Deemos Technology, China
 CHUXIAO ZENG*, ShanghaiTech University, China and Deemos Technology, China
 QIXUAN ZHANG*, ShanghaiTech University, China and Deemos Technology, China
 HONGYANG LIN, ShanghaiTech University, China and Deemos Technology, China
 RUIXIANG CAO, ShanghaiTech University, China and Deemos Technology, China
 WEI YANG, Huazhong University of Science and Technology, China
 LAN XU, ShanghaiTech University, China
 JINGYI YU, ShanghaiTech University, China



Fig. 1. Our learning-based approach generates video-driven neural physically-based facial asset for realistic production. Our pipeline supports both high-fidelity facial capture and cross-identity facial motion retargeting, and enables various highly realistic physically-based effects including geometry and material editing. Top: photo-realistic rendering results of different neural physically-based facial asset with stylized appearance. Bottom: cross-identity video-driven results from novel view.

Production-level workflows for producing convincing 3D dynamic human faces have long relied on a disarray of labor-intensive tools for geometry

*Equal contribution.

Authors' addresses: Longwen Zhang, ShanghaiTech University, Shanghai, China, Deemos Technology, China, zhanglw2@shanghaitech.edu.cn, zhanglw@deemos.com; Chuxiao Zeng, ShanghaiTech University, Shanghai, China, Deemos Technology, China, zengchx@shanghaitech.edu.cn, zengchx@deemos.com; Qixuan Zhang, ShanghaiTech University, Shanghai, China, Deemos Technology, China, zhangqx1@shanghaitech.edu.cn, zhangqx@deemos.com; Hongyang Lin, ShanghaiTech University, Shanghai, China, Deemos Technology, China, linhy@shanghaitech.edu.cn, linhy@deemos.com; Ruixiang Cao, ShanghaiTech University, Shanghai, China, Deemos Technology, China, caorx@shanghaitech.edu.cn, caorx@deemos.com; Wei Yang, Huazhong University of Science and Technology, Wuhan, China, weiyangs@hust.edu.cn; Lan Xu, ShanghaiTech University, Shanghai, China, xulan1@shanghaitech.edu.cn; Jingyi Yu, ShanghaiTech University, Shanghai, China, yujingyi@shanghaitech.edu.cn.

and texture generation, motion capture and rigging, and expression synthesis. Recent neural approaches automate individual components but the corresponding latent representations cannot provide artists explicit controls as in conventional tools. In this paper, we present a new learning-based, video-driven approach for generating dynamic facial geometries with high-quality physically-based assets. Two key components are well-structured latent spaces due to dense temporal samplings from videos and explicit facial expression controls to regulate the latent spaces. For data collection, we construct a hybrid multiview-photometric capture stage, coupling with an ultra-fast video camera to obtain raw 3D facial assets. We then set out to model the facial expression, geometry and physically-based textures using separate VAEs where we impose a global multi-layer perceptron (MLP) based expression mapping across the latent spaces of respective networks, to preserve characteristics across respective attributes while maintaining explicit controls over facial geometry and texture generation. We also introduce to

model the delta information as wrinkle maps for the physically-base textures in our texture VAE, achieving high-quality 4K rendering of dynamic textures. We demonstrate our approach in high-fidelity performer-specific facial capture and cross-identity facial motion transfer and retargeting. In addition, our multi-VAE based neural asset, along with fast adaptation schemes, can also be deployed to handle in-the-wild videos. Besides, we motivate the utility of our explicit facial disentangle strategy by providing various promising physically-based editing results like geometry and material editing or wrinkle transfer with high realism for production. Comprehensive experiments show that our technique provides higher accuracy and visual fidelity than previous video-driven facial reconstruction and animation methods.

CCS Concepts: • Computing methodologies → Motion capture.

Additional Key Words and Phrases: Physically-Based Face Rendering, Facial Modeling, Digital Human, Video-Driven Animation

1 INTRODUCTION

High-quality and realistic digital avatars have been increasingly deployed in feature films, game productions, entertainment industry, and most recently immersive experiences in the Metaverse. Despite tremendous advances on modeling human body [Loper et al. 2015], producing 3D dynamic faces remains as a challenging problem to computer vision and computer graphics: we humans are extremely sensitive to the perception of facial idiosyncrasies where even slightest inconsistency can be easily detected.

Production-level workflows for generating compelling and convincing dynamic virtual character involve a disarray of tasks, ranging from generating realistic geometry and physically-based appearance attributes (e.g., diffuse albedo, specular intensity, roughness, normal map and displacement) [Li et al. 2020a], to capturing and modeling fine-grained facial motions [Laine et al. 2017], and to transferring the corresponding motions to new performers with different physiognomy or performing a wide range of expressions [Thies et al. 2016]. Geometry and appearance data are commonly acquired using elaborately designed capture systems such as a Light Stage [Debevec et al. 2000] or a multi-camera dome [Joo et al. 2017], to faithfully reproduce how light interacts with facial tissues. Once collected, the rich raw data then undergoes time-consuming manual post-processing, often by a professional production team, where highly skilled artists need to carefully adjust both the physically-based textures and the facial expression models, following the Facial Action Coding System (FACS) [Ekman and Friesen 1978]. Such a pipeline is clearly too expensive (in both cost and time) to be deployed to support a broader audience, e.g., to create an avatar for everybody. There is an urgent demand to develop more automatic workflow to at least reduce, if not fully eliminate, the tedious manual labors in the production cycle.

Recent deep learning techniques [Lattas et al. 2021; Li et al. 2020b,a] have shown hopeful results to enable automated facial asset generation direct from the captured data with little human intervention, bringing huge potential to revolutionize production-level workflows. In particular, the data-driven strategy employed by learning-based techniques is applicable to handle datasets of different scales, as big as thousands of subjects for producing a generic model or as small as a single subject with different expressions and lighting conditions for portrait animation. For the former, generic models [Bao et al. 2021; Feng et al. 2021; Li et al. 2020b, 2017; Raj et al. 2021]

can achieve high robustness despite environment lighting changes and variations in facial geometry, motion or even physically-based attributes. The notable framework [Li et al. 2020b] manages to learn personalized blend shapes along with pore-level dynamic physically-based texture maps whereas latest advances [Bao et al. 2021] can further generate riggable head models with high-resolution albedo and normal maps. Their generated assets are directly usable to existing production pipelines for producing facial animations and photo-realistic rendering. A major challenge there though is that they highly rely on blend shapes for explicit control which can easily lead to loss of fine-grained details in both facial expressions and dynamic physically-based textures. By far latest neural generic models still cannot match the quality required by production-level applications for synthesizing facial idiosyncrasies of an unseen subject.

For the latter, performer-specific neural models can produce both geometry and appearance with extremely fine details. For example, emerging neural rendering approaches [Gafni et al. 2021; Lombardi et al. 2019, 2021; Wei et al. 2019] can conduct compelling end-to-end facial rendering at photo-realism. However, unlike the generic model that provides explicit controls, controlling fine details in geometry, motion or physically-based textures remains unresolved, preventing their seamless integration into existing production pipelines for games or feature films. To partially address this challenge, recent work [Cao et al. 2021; Lombardi et al. 2018] utilize the conditional variational autoencoder (CVAE) framework [Kingma and Welling 2014] and acquire fine geometry and view-dependent texture maps as intermediate results which serve as byproducts for facial reconstruction in post-production. Various subsequent work [Chen et al. 2021; Ma et al. 2021; Yoon et al. 2019] have enabled fine-grained performer-specific facial capture, even relightable animations [Bi et al. 2021], and even transfers across different identities and characters [Moser et al. 2021]. Despite their effectiveness, these methods still fall short of explicitly providing physically-based facial textures directly deployed to traditional production-level workflows, undermining their applicability in realistic and controllable digital face modeling.

In this paper, we present a new learning-based, video-driven approach for generating dynamic facial geometries with high-quality physically-based textures such as pore-level diffuse albedo, specular intensity and normal map for performer-specific production. Our approach supports both high-fidelity performer-specific facial capture and cross-identity facial motion retargeting. In particular, it is directly applicable for producing various highly realistic physically-based effects such as geometry and material editing, wrinkle transfer, etc, as shown in Fig. 1.

Using videos, instead of separate shots, to produce physically-based facial assets imposes several challenges. On the data front, by far there are very few high-quality 3D facial video datasets publicly available. On the processing, tailored, neural modeling algorithms need to be elaborately designed to handle the spatial-temporal data. On editing, companion tools should be developed to support production. To address these issues, we first construct a tailored multi-view photometric capture stage for capturing fast facial motions that we call FaStage. Different from existing capture systems aimed at static or slow facial motions such as the USC Light Stage [Debevec

et al. 2000], FaStage uses a coordinated high-speed camera system in addition to a dense set of space- and time-multiplexed illumination array. Coupled with ultra-fast video cameras (Flex4K), we can capture dynamic facial physically-based assets of a performer at 24 frame-per-second (fps). Using photometric reconstruction, FaStage produces a sequence of high quality 3D model stored as 4D topology-consistent facial geometry sequences along with per-frame physically-based texture assets for each performer. Next, inspired by recent work [Lombardi et al. 2018; Moser et al. 2021] we adopt Variational Autoencoder (VAE) [Kingma and Welling 2014] to train a unified neural representation of our dynamic facial assets, which maintains a well-structured latent space so that the trained results can be applied to various video-driven facial applications. Specifically, we set out to model the facial expression, geometry and physically-based textures using separate VAEs where we impose a global MultiLayer Perceptron (MLP) based expression mapping across the latent spaces of respective networks. This allows us to preserve characteristics across respective attributes using a single framework. To train the expression VAE from the RGB video footage, we explicitly disentangle the latent space into expression and viewpoints. For the geometry VAE, we first convert the recovered geometry sequence into topology-aligned geometry images [Li et al. 2020a]. To train on the geometry images, we introduce a virtual head pose argumentation strategy within the latent space formulation, to enable robust facial geometry inference against errors in head pose estimation across captured sequences. For the physical-based texture VAE, we connect the latent space to facial expression for conducting view-independent texture inference. In addition, we explicitly decode the discrepancies on top of the neutral textures to produce wrinkle maps, which are critical for producing and editing photo-realistic 4K dynamic textures. We further introduce a multi-stage training scheme to train all VAEs and our MLP-based mapping across latent spaces.

A unique advantage of our technique over prior neural approaches is that, one can directly apply facial expression driven animations to the resulting performer-specific neural asset, and generates high-quality face geometries with pore-level dynamic physically-based textures. So that, the results can be seamlessly integrated into production-level physically-based rendering, and for the first time, to directly process a video sequence instead of individual models. Our multi-VAE based neural asset, along with a fast adaptation scheme, can also be deployed in-the-wild videos to produce cross-identity, fine-grained facial animations. Finally, the explicit disentanglement of different facial attributes enables convenient geometry and material editing for post production, such as animating stylized characters at high realism.

To summarize, our main contributions include:

- We present a novel neural facial asset generator for producing personalized dynamic facial geometries with pore-level physically-based textures. Specifically, we obtain the training data using a multi-view photometric capture stage called FaStage that can capture dynamic 3D facial geometry of 4K resolution at 24 fps.
- We design a novel multi-VAE design tailored for our input geometry and texture sequences from videos, where individual

VAEs aim to disentangle facial attributes across expression, geometry and texture, and a global mapping MLP representing facial express is used to correlate the latent spaces.

- Once trained, our neural facial assets can be used on in-the-wild video sequences to produce cross-identity neural facial animations with ultra high realism. We can further edit the disentangled attributes to refine geometry or materials and to transfer details such as wrinkles.

2 RELATED WORKS

Facial Animations. Facial animation is usually based on the 3D head shape regression or the detection of landmarks to construct a parametric model of the face [Blanz and Vetter 1999; Ekman and Friesen 1978]. Blendshape is a prevalent parametric model in the industry and artists usually need to manually split or adorn the expressions to allow further recreation and animation [Lewis et al. 2014]. For a real performer, we can register a template model to its scan for different expressions to generate pre-defined blendshapes like FaceWarehouse [Cao et al. 2014] and 3D morphable model [Egger et al. 2020]. Alternatively, Weise et al. [2011] propose to fit the dynamic geometry of face with pre-defined models for RGBD input, while Bao et al. [2021] enable high-fidelity digital avatar generation with RGB-D video input. Besides, numerous strategies have been proposed in the literature to address the challenge of reconstructing a 3D face from a single input image [Cao et al. 2013; Guo et al. 2020, 2018; Paysan et al. 2009; Richardson et al. 2016; Tuan Tran et al. 2017].

Compared with the classical 68-landmark-based reconstruction [King 2009; Zhang et al. 2014], Li et al. [2017] train the FLAME model with a large amount of 4D scans and achieved impressive accuracy in capturing facial performance from video. To enhance reconstruction with facial details, Cao et al. [2015] optimize their previous work by adding high-fidelity facial detail to low-resolution face tracking data. There are also works that successfully handle extreme skin deformation [Chen et al. 2019; Wu et al. 2016]. DECA [Feng et al. 2021] further improve FLAME [Li et al. 2017] by additionally predicting individual-specific animatable details. High-fidelity facial details from real performers can be added to scanned facial models. Laine et al. [2017] build an performer-specific framework for production. As the network converges to the individual and is set in advance to use the high precision facial model for constructing the PCA basis, their method improves accuracy and benefits higher-precision industry production. The method of Olszewski et al. [2016] is capable of processing several different identities within limited viewpoints under VR/AR headsets. Moser et al. [2021] apply image-to-image translation on the input video and render CG sequence in order to extract a common representation of expression for both before decoding the latent vector into the weights of the target character’s PCA blendshapes. For comprehensive reviews on facial animations, we refer the readers to [Morales et al. 2021] and [Zollhöfer et al. 2018]. Compared to previous works, our method can express facial features at a more detailed level with the aid of physically-based dynamic texture assets.

Physically-based Texture Generation. Physically-based textures, such as diffuse albedo, normal maps, specular maps and displacement maps, serve as vital ingredients in the process of creating photo-realistic digital avatars. Ma et al. [2007] pioneer using gradient illumination and diffuse-specular separation with polarizers to acquire high-fidelity physically-based textures. By changing the arrangement of linear polarizers, Ghosh et al. [2011] successfully adapt the previous method to a multiview setting. To support dynamic expressions, Fyffe et al. [2011] use Phantom v640 high-speed cameras to achieve facial performance capture in 264 fps. Fyffe and Debevec [2015] use color polarized illumination setup to enable texture scanning in a single shot. LeGendre et al. [2018] modify the camera setting to mono camera to achieve more efficient and higher-resolution results. In human performance capture, Guo et al. [2019] combine spherical gradient illumination with volumetric captures to produce compelling photorealism. With the advances in deep learning, possibilities of estimating the parameters of a predefined reflectance field from single image input [Huynh et al. 2018; Saito et al. 2017; Yamaguchi et al. 2018] have been demonstrated.

Compared with the gradient method, passive facial capture has also made significant progress in recent years, largely attributed to the open-source and commercial multi-view reconstruction software [Beeler et al. 2010]. By including skin parameters such as skin color and variations in hemoglobin concentration, Gotardo et al. [2018] manage to obtain even more detailed facial features. However, in general, data produced by such passive capture methods still cannot match the photometric one due to calibration errors, camera resolutions, reconstruction errors, etc.

There are also emerging approaches that employ generative adversarial networks (GANs) to synthesize or infer textures of competent quality for industrial uses. Li et al. [2020a] introduce a framework to generate geometry and physically-based textures from identity and expression latent spaces. They further apply super-resolution networks to produce textures that contain pore-level geometry. Lattas et al. [2021] manage to infer renderable photorealistic 3D faces from a single image. Since facial animation corresponds to a series of 3D scans, we can predict blendshapes from a single 3D scan of the neutral expression of the performer and then infer dynamic texture maps in a generative manner based on expression offsets [Li et al. 2020b]. Differently, we build dynamic textures using wrinkle maps, which allows us to maintain the authenticity of the high-resolution textures while avoiding the artifacts generated by super-resolution networks.

Deep Face Models. There is an emerging trend on replacing classical geometry and texture-based models with deep models. A neural network can potentially extract a latent vector from image input and later decode it into high-quality mesh and textures. Lombardi et al. [2018] use a variational autoencoder (VAE) to encode geometry and view-dependent texture information. They then applied domain adaptation techniques to achieve real-time reenactment of a textured avatar with VR headset’s multi-camera input. Yoon et al. [2019] utilize the model proposed by Lombardi et al. [2018], forcing the encoder to maintain temporal consistency of facial landmarks and textures. Their model is capable of handling monocular input images under uncontrolled lighting environments. Cao et al. [2021]

further estimate a gain map and a bias map to additionally improve rendering.

GAN-based methods [Gecer et al. 2019; Lattas et al. 2021; Li et al. 2020a] separate the shape and expression or using photorealistic differentiable rendering-based training to enhance details in model generation. Other identity-agnostic methods [Abrevaya et al. 2020; Burkov et al. 2020; Nirkin et al. 2019] aim to enhance the identity-independence by imposing constraints in the latent space. Feng et al. [2018] introduce UV-position map for 3D geometry representation to enable better regression of CNN. Bi et al. [2021], on the other hand, build a deep face model capable of producing OLAT textures, making the predicted avatar relightable under novel lighting environments. In our work, we further improve the quality and editability of the deep face models by generating physically-based textures, thanks to the high-quality dynamic facial assets we captured.

3 NEURAL PHYSICALLY-BASED FACIAL ASSET

The panoptic facial assets, i.e., face geometry and physically-based texture (including diffuse albedo, normal map, and specular intensity), under various facial expressions and lighting conditions, are essential for production-level face rendering and animation. However, capturing the entire span of facial assets is impossible even for the most advanced face performance capture system, such as the Light Stage, due to the varieties of human facial expressions. Moreover, tremendous labor of manual post-processing is required to carefully adjust both the physically-based texture assets and the facial expression models.

As illustrated in Fig. 2, instead of explicit modeling, we present a neural representation of the performer-specific facial asset, which supports the generation of dynamic facial geometries with high-quality physically-based texture for performer-specific production. Our neural physically-based facial asset learns latent for facial expression, geometry and texture separately (we use ‘texture’ to shorten ‘physically-based texture’) via a novel triplet supervision scheme. Face geometry and texture with novel expression can be easily inferred from our network. With this representation, we can render the face from novel viewpoints, environmental lighting, and edit its physical properties with minimum effort. We can also drive the performer-specific neural facial assets with an in-the-wild video of facial performance or even drive a new character with different geometry and texture. To produce physically-based facial assets for training, we construct a face performance capture system called “FaStage”, which adopts the core concept from the USC Light Stage, with modified high-speed camera systems to better capture the span of facial assets.

4 DYNAMIC FACIAL ASSET ACQUISITION

To construct a performer-specific neural facial asset for product-level rendering, we need the facial geometry and physically-based texture under various expressions and lighting for neural optimization. The most renowned face performance capture system is the USC Light Stage [Debevec et al. 2000], which exploits the time multiplex lighting for facial texture recovery. The Light Stage system recovers the face reflectance field at unprecedented high quality. The original Light Stage system uses DSLR cameras to recover the

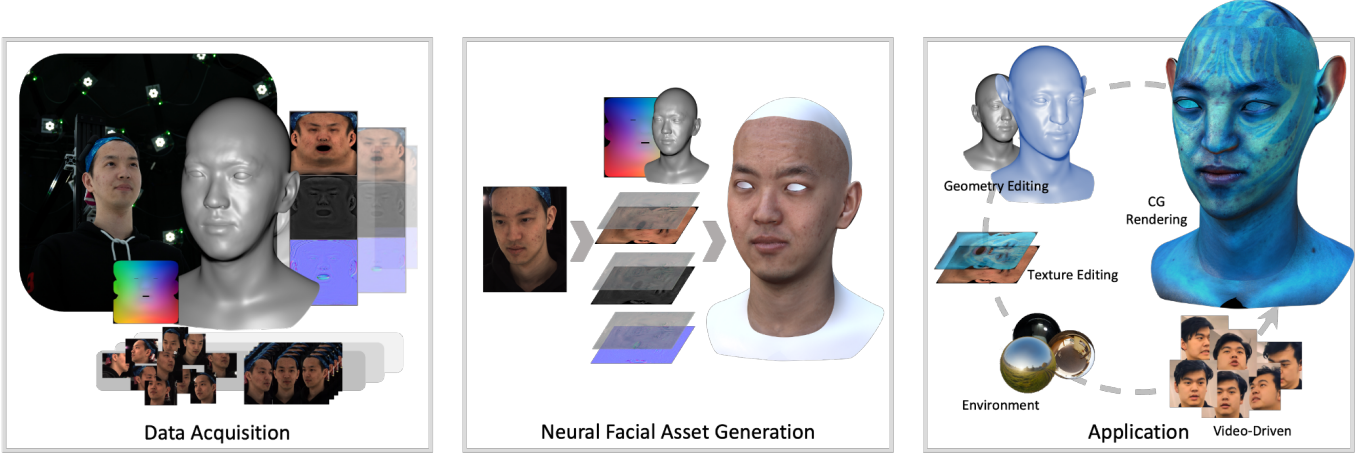


Fig. 2. **The algorithm pipeline of our approach for neural physically-based facial asset generation.** Our fast capture stage (FaStage) extends the classical photometric LightStage [Debevec et al. 2000]. FaStage combines multi-view reconstruction and photometric reconstruction to recover the dynamic geometry and physically-based textures of a performer frame by frame. We then present a new neural representation with tailored network designs and training strategies to model dynamic meshes and textures under different expressions. The trained neural assets can be used for a range of applications, including appearance stylization and relighting under novel expressions and viewpoints.

facial texture assets, which may be problematic for our task as we aim to learn the latent space of expression, geometry and textures, where sufficient observation is essential. We adopt a similar hardware structure but add three ultra-high-speed cameras (can capture at 1kHz) to recover facial textures at 24 fps. Such per-frame facial texture is the key for effectively training of our neural facial asset.

4.1 The FaStage

We adopt a similar semi-dome structure for our FaStage capture system as the Light Stage, where space-and-time-multiplexed light-emitting diodes (LEDs) are evenly mounted on the semi-dome. Distinctively, we replace the DSLR cameras with two sets of camera systems, one set of ultra-high-speed cameras run at 1000 fps and the other of machine vision cameras at 24 fps, to capture a performer’s per-frame facial appearance and motion with extremely high precision. Figure 4 shows the architecture of our capture system, which consists of 146 polarized LED units, 3 high-speed cameras, and 24 machine vision cameras. The cameras and LEDs are synchronized by an external signal generator.

high-speed Cameras. Our FaStage adopts two sets of camera systems, one high-speed camera system for photometric stereo and the other set of machine vision cameras. We mount three PHANTOM Flex4K-GS high-speed cameras for the high-speed camera system, which captures 4K images at 1000 FPS according to a global shutter. We equip each high-speed camera with a ZEISS CP.3 135mm lens and a linear polarizer. Also, to recover face geometry at high precision, we additionally place 24 machine vision cameras, which capture 5.3MP images at 50 FPS. We set the Flex4K cameras’ capture frequency at 912 Hz and the machine vision cameras’ at 24 Hz. For every face geometry reconstructed at 1/24 second using machine vision cameras, we exploit the 38 images captured under various

lighting during the interval and recover facial texture using photometric stereo.

Light Units. We install 146 customized 2-directional polarized light units distributed evenly in our Light Stage dome. Each light unit consists of 6 high brightness light-emitting diodes (LEDs) and a customized programmable control board. Each LED on a light unit belongs to one of the two orthogonal polarization groups, and we use the same polarization direction arrangement as Ghosh et al. [2011]. A high-power LED driver on the control board controls each polarization group individually, which is capable of toggling the LEDs at frequency up to 500 kHz. This configuration allows the system to produce polarized gradient illumination patterns at very high frame rate. Circuits of the two LED driver sets for polarization groups are controlled by a System on a Chip (SoC), which is capable of rapidly alternating the brightness of two LED groups at frequency up to 1kHz.

Storage. Recall that we utilize two sets of cameras in our system. For the high-speed cameras, which run at 4K resolution, 12bit depth and 912Hz, we save captured raw data into a superspeed RAM inside the camera and then transfer the data into a portable SSD after the capture is finished. For machine vision cameras, which run at 2K resolution, 8bit depth and 24Hz. We transfer the raw, uncompressed data into high performance servers through CXP-6 recorders and subsequently save into storage servers.

Synchronization. To make the two sets of camera system work coherently, we set two phase-synchronized control signals in our systems. One signal controls three 10MP high-speed cameras and 146 polarized LED units and works at 912Hz. The other controls

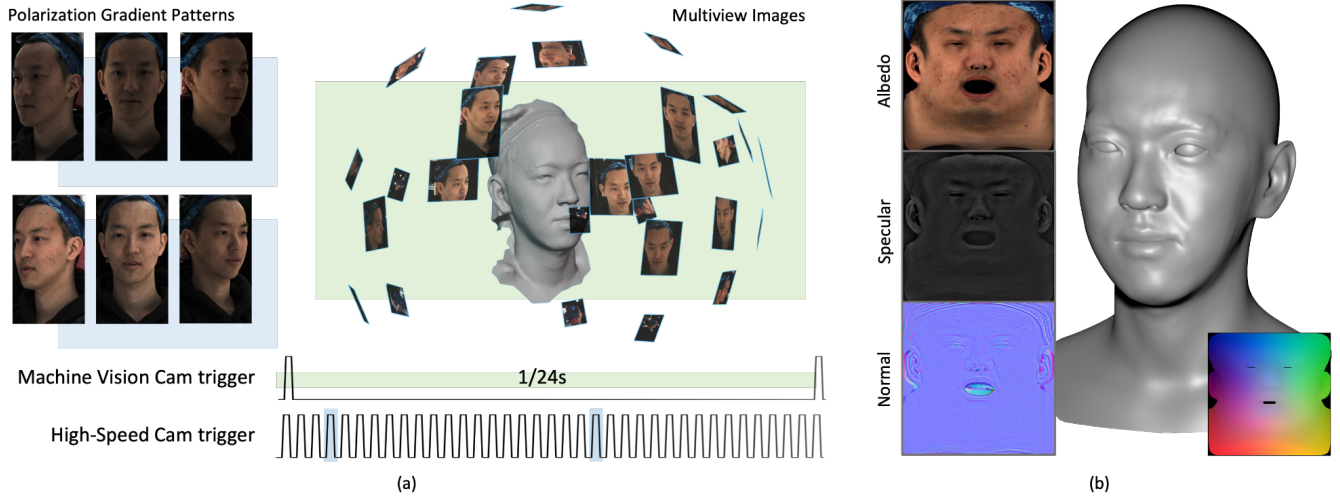


Fig. 3. **Illustration of our data acquisition pipeline.** We utilize three high-speed cameras to capture polarization gradient patterns for dynamic physically-based texture acquisition. Multiple machine vision cameras are synchronized at a low frequency for dynamic facial geometry acquisition.

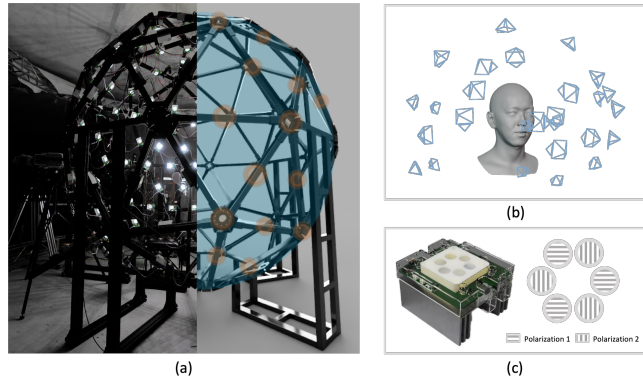


Fig. 4. **Illustration of our capture system.** (a) Light Stage capture system and the layout of LED units, (b) Layout of machine vision cameras, (c) Polarized LED unit. The Light Stage consists of 146 2-directional polarized LED units. Each of them is controlled by an individual SoC and has two groups of high-power LEDs with polarization directions perpendicular to each other.

the rest 24 5MP machine vision cameras and works at 24Hz. The two control signals are generated from the same external signal generator in a phase-synchronized manner. The 912Hz control signal is fed simultaneously into three high-speed cameras and the light controller, and the light controller broadcasts signal to all light units through the daisy-chained network. For 24Hz low-frequency control signal, it's fed into the recorders of the storage servers. The recorders then trigger all the connected machine vision cameras.

4.2 Facial Asset Collection

Due to the varieties of face expressions and movements, it's impossible to capture the full span of facial asset. Our intent is to collect facial asset for typical face movements, and exploit deep networks

to naturally bridge the gaps in sparse facial asset observations. We capture a total of 5 minutes of face performance for each performer at 24 fps and acquire the corresponding facial assets. We ask each performer to give the following performances: a short speech, exaggerated expressions of different emotions, extreme expressions like squeezing the eyes or opening the mouth widely, and continuous movements of cheek, eyebrows, mouth and jaw. We additionally capture one **neutral frame** where the performer shows no expression as the reference frame. We aim to retrieve the high-quality dynamic facial assets, including the face geometry, diffuse albedo, specular intensity and normal map, from data captured by FaStage for optimizing our neural assets representation.

Dynamic Facial Assets. During the capture process, we send one specific type of control signal to turn all lights on and collect both the machine vision camera and high speed camera images. Then we perform the multi-view stereo technique [Seitz et al. 2006] on synchronized images with full light on collected by both the machine vision cameras and high-speed cameras to extract the face geometry. We also fit a human face model Li et al. [2020a] to our recovered geometry using the optical flow and ICP algorithms [Rusinkiewicz and Levoy 2001]. We then can represent the face geometry with UV maps and uniformly sample 256×256 points where each pixel represents the location of corresponding point on mesh, similar to Li et al. [2020a], and generate geometry maps for network training. For physically-based textures, we apply a total number of 38 gradient illumination patterns for every 1/24 second, similar to the patterns in Wilson et al. [2010]. And we then use the 38 images from high-speed cameras under the corresponding gradient illumination patterns to recover diffuse albedo, specular intensity and object-space normal map using the photometric stereo technique [Ma et al. 2007] at 24 FPS. Finally, we merge the corresponding texture across different views in UV space using the method in Ghosh et al. [2011].

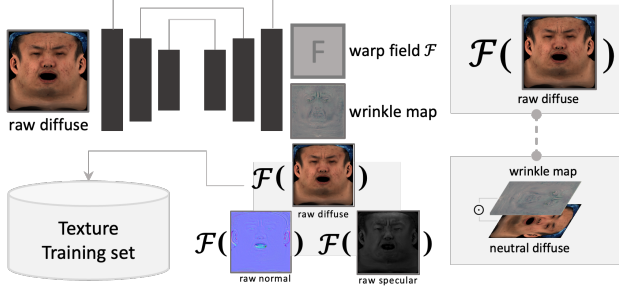


Fig. 5. **Pipeline of texture stabilization.** We utilize an unsupervised method to predict the warp field with regard to the neutral textures for textures of each frame. Stabilized textures, which are produced by applying the warp field to the textures of each frame, will be used as training data.

To further reduce temporal noise, we transform the object-space normal maps into tangent space. Specifically, we first apply the object-space normal map to the face geometry and then use the resulting high-poly geometry and a low-poly geometry to bake the tangent-space normal map.

Temporal Stabilization. Since we adopt a multi-view setup and merge textures across different views, it suffers temporal instability due to small spatial discrepancy. To produce temporally stable textures for network training, we develop an unsupervised approach. As illustrated in Fig. 5, we use a U-Net to predict a warp field and a wrinkle map for textures in frame with regard to the neutral frame. We observe normal maps contains some noises, and the subtle details in diffuse albedo it most suitable for aligning temporal frames. Hence we only use the diffuse albedo for temporal stabilization. Given an input diffuse albedo T_t at t -th frame, our stabilization network Φ predicts both a warp field \mathcal{F}_t and a corresponding wrinkle map \mathcal{W}_t :

$$\mathcal{F}_t, \mathcal{W}_t = \Phi(T_t), \quad (1)$$

where \mathcal{F}_t represents pixel-wise flow and we use $\mathcal{F}_t(\cdot)$ to represent the warping of a texture to neutral frame where the performer makes no expressions. We expect to obtain an temporally aligned diffuse albedo after applying warp field \mathcal{F}_t to T_t . Here we develop the following fidelity loss:

$$\mathcal{L}_{fid} = \|\mathcal{F}_t(T_t) - \mathcal{W}_t \odot N\|_1, \quad (2)$$

where N is the neutral diffuse albedo and \odot is element-wise multiplication. Then, we use a temporal consistency term to ensure texture stability between consecutive frames. Given the network output $\mathcal{W}_t, \mathcal{W}_{t+1}$ from consecutive frames, our temporal loss is formulated as

$$\mathcal{L}_{tem} = \|\mathcal{W}_t - \mathcal{W}_{t+1}\|_1, \quad (3)$$

which implicitly aligns the two textures. In addition, we apply a regularization term to restrict the flow within a reasonable distance, as:

$$\mathcal{L}_{dis} = \|\mathcal{F}_t\|_2 + \|\nabla \mathcal{F}_t\|_2. \quad (4)$$

Our total loss for texture stabilization is formulated as follows:

$$\mathcal{L}_{stab} = \mathcal{L}_{fid} + \mathcal{L}_{tem} + \mathcal{L}_{dis}. \quad (5)$$

where weights for balancing different losses are omitted for simplicity in presentation. The diffuse albedo, specular intensity and normal map share the same warp field, therefore we apply \mathcal{W} to all the other textures similar to the diffuse albedo. This bi-directional approach significantly improves the temporal stability of textures and helps the generation of neural facial assets. We use all captured dynamic textures to optimize \mathcal{L}_{stab} for training Φ . Then, we apply Φ to process all textures and align them to a neutral frame as preprocessing.

5 NEURAL FACIAL ASSET GENERATION

From captured dynamic facial assets of a specific performer, we intend to transform it into a drivable neural representation. Traditional human face performance capture adopts a mesh or parametric model based representation, and relies on heavy manual labor for align geometry and textures, rigging and expression deformation. This tedious process can be potentially bypassed by a neural based approach. Notice for human face performance capture, it is essential to drive the face animation according to certain expression. Here we use a triplet supervision approach to effectively separate expression, geometry and texture latents. To this end, we build a learning framework with three networks for disentangling the expression, face geometry and physically-based texture. The expression latents are then mapped to the geometry and texture latents for decoding into corresponding geometry and texture for rendering. The whole training pipeline is illustrated in Fig. 6

In the first stage, we specifically train a variational autoencoder (VAE) to encode the expression from an input frame. We propose a novel triplet training scheme to disentangle the face expression and viewpoint information. Specifically, we enforce the VAE to learn separate latents by sampling the dataset according to expression and viewpoint equivalent, and force the combination of expression and viewpoint latents to generate the correct image. Similarly, we also use a VAE to encode the face geometry and texture. During triplet training, we also send the head pose estimated from data acquisition to the network for better handling head pose variance. During inference, our system predicts geometry and textures with encoded expression, which generates the information we needed for rendering the captured performer’s avatar. Notice in this section, all data mentioned is sampled from the preprocessed FaStage data, i.e., geometry, diffuse albedo, specular intensity and normal map, of the same performer, i.e., our neural facial asset is performer specific.

5.1 Expression and Viewpoint Disentanglement

We train a VAE to learn a global representation for expressions and viewpoints from training footage, as illustrated in Fig. 7. Given an input image I from view i at frame t , our expression encoder \mathcal{E}_e encodes it to an expression latent Z_e and a viewpoint latent Z_v , while our expression decoder \mathcal{D}_e predicts the reconstructed image \hat{I} given these two latents. To ensure latent space consistency between the encoder and decoder, we predict cycled latents \hat{Z}_e, \hat{Z}_v , ($\hat{Z} = \mathcal{E}[\mathcal{D}(Z)]$), from reconstructed image \hat{I} , and adopt the reconstruction and latent consistency loss.

$$\mathcal{L}_{rec} = \|I - \hat{I}\|_1, \quad \mathcal{L}_{cyc} = \|Z_e - \hat{Z}_e\|_2 + \|Z_v - \hat{Z}_v\|_2 \quad (6)$$

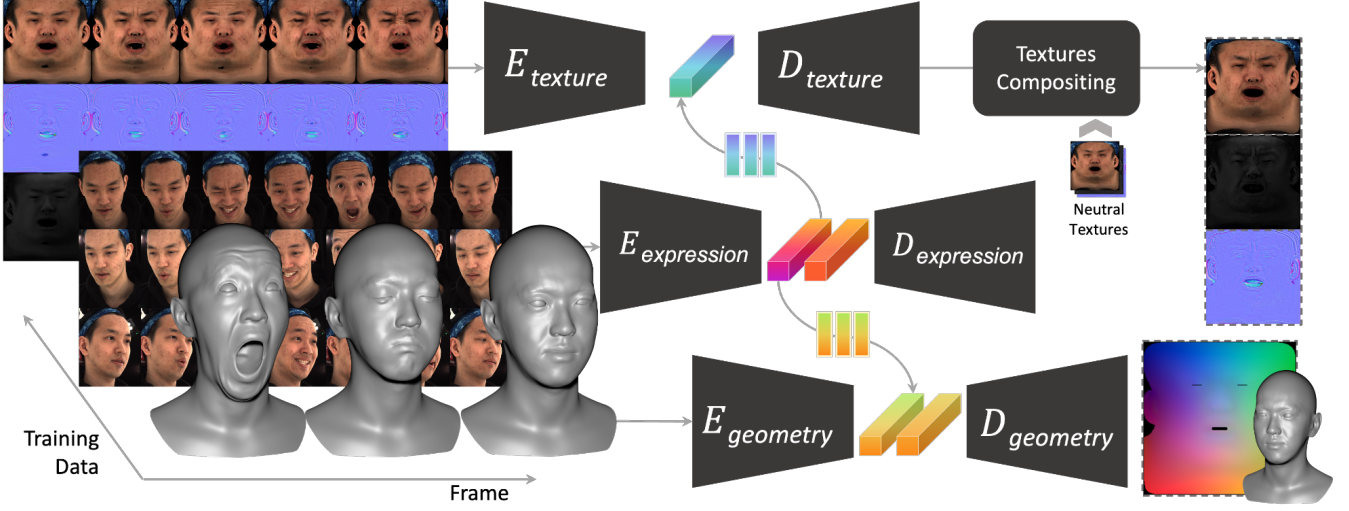


Fig. 6. **Neural physically-based facial asset.** For each frame, the training input consists of multi-view facial images captured in FaStage, as well as coarse geometry and physically-based textures. Our approach trains three deep Variational Auto-Encoders to obtain three latent space separately on captured image, geometry and textures. Then two multilayer perceptrons are trained for latent space translation from image to geometry and textures.

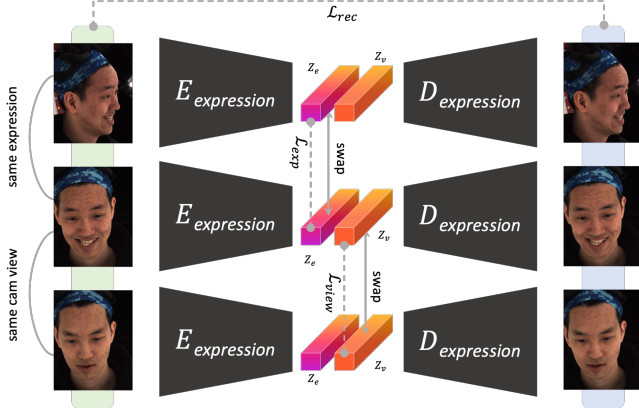


Fig. 7. **Architecture of expression network.** To better extract expression features from input images, we constrain the encoder to output the same expression latent from images with the same expression, and same view latent from images under the same view. The extracted latents are then swapped with each other and fed into decoders. We minimize the reconstruction loss of decoded images.

Notice we omit view and frame index i and t in the equation for simplicity in presentation.

Triplet supervision for expression encoding. We designed a triplet training scheme that focuses on retrieving consistent expression and viewpoint information across views and frames. In each training iteration, we randomly pick two frames s, t , and two random views i, j . Notice all frames and views data are from the same performer. Given the input images $I^{t,i}, I^{t,j}, I^{s,i}$, our encoder E_e predicts the performer's expressions and the camera's viewpoint latents for each of them, i.e., $Z_e^{t,i}, Z_e^{t,j}, Z_e^{s,i}$: Notice the performer exhibits

the same expression in $I^{s,i}$ and $I^{s,j}$, while in $I^{s,i}$ and $I^{t,i}$, the viewpoints are the same. Therefore, we minimize the distance between expression latent and view latent to achieve expression-viewpoint disentanglement:

$$\mathcal{L}_{exp} = \|Z_e^{t,i} - Z_e^{t,j}\|_2, \quad \mathcal{L}_{view} = \|Z_v^{t,i} - Z_v^{s,i}\|_2 \quad (7)$$

Besides constraining the encoder, we want the decoder to focus on recovering the expression despite the disturbances from viewpoint changes. Therefore, the subsequent reconstruction is done in a cross frame and view manner:

$$\begin{aligned} \tilde{I}^{t,i} &= \mathcal{D}_e(Z_e^{t,i}, Z_v^{s,i}) \\ \tilde{I}^{t,j} &= \mathcal{D}_e(Z_e^{t,j}, Z_v^{s,i}) \\ \tilde{I}^{s,i} &= \mathcal{D}_e(Z_e^{s,i}, Z_v^{t,i}) \end{aligned} \quad (8)$$

The decoded result $\tilde{I}^{t,i}$ should be the same as the original image $I^{t,i}$, since the encoded expression and viewpoint information are supposed to be the same. The corresponding reconstruction error at this stage is formulated as:

$$\mathcal{L}_{cro} = \|I^{t,i} - \tilde{I}^{t,i}\|_1 + \|I^{t,j} - \tilde{I}^{t,j}\|_1 + \|I^{s,i} - \tilde{I}^{s,i}\|_1. \quad (9)$$

Then the total loss for our expression network can be formulated as follows:

$$\mathcal{L}_E = \mathcal{L}_{rec} + \mathcal{L}_{cyc} + \mathcal{L}_{exp} + \mathcal{L}_{view} + \mathcal{L}_{cro}. \quad (10)$$

This loss helps us to constrain Z_e so that it contains only the expression features, and the viewpoint information is in Z_v . Notice we omit balancing weights for simplicity in presentation.

5.2 Geometry Extraction

Recall that we represent the facial geometry with a 2D-geometry map in UV space where each pixel represents the 3D coordinate of corresponding vertex. Therefore, we can regard the geometry

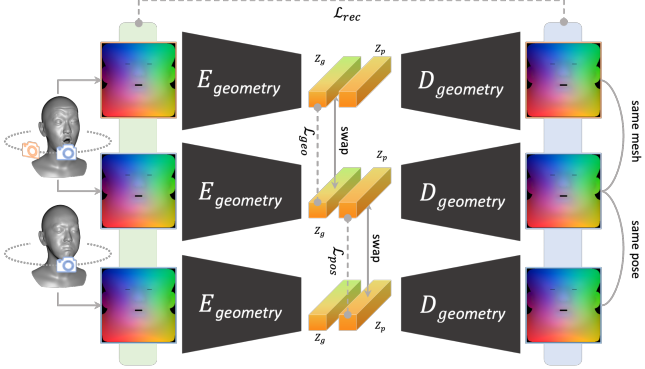


Fig. 8. **Architecture of geometry network.** To better understand the geometry and eliminate the pose errors between multiple scanned clips, we constrain the encoder to output the same geometry latent from geometries with the same expression, and the same pose latent from geometries under the same pose. Note the geometries used for training have been augmented with random rotations and translations. The extracted latents are then swapped with each other and fed into decoders. We minimize the reconstruction loss of the decoded geometries.

inference as an image reconstruction task. To extract better geometry features and eliminate the minor head pose errors, we adopt a similar network structure to the one developed for expression encoding. For improving robustness, we apply random rotations and translations to scanned geometries for data augmentation. As illustrated in Fig. 8, given an input geometry map G from frame t with augmentation operation a , our geometry encoder E_g encodes it to a geometry latent $Z_g^{t,a}$ and a pose latent $Z_p^{t,a}$, while our geometry decoder D_g predicts the reconstructed image $\hat{G}^{t,a}$ given these two latent. Similar to the expression disentanglement, we randomly pick frames with s, t and augmentation operations a, b for training. Note that we choose s, t from the same dynamic clip and make sure they are temporally close to ensure both geometries without augmentation have similar poses. Specifically, when we fix geometry latent and change pose latent, the geometry maps generated by the decoder should exhibit similar geometry and only differ in rotation and translation. Therefore, the decoding process itself is designed to be independent from the pose latent, which could be formulated as:

$$\mathcal{D}_g(Z_g, Z_p) = M_p(Z_p) \otimes \mathcal{D}_g^\dagger(Z_g), \quad (11)$$

where M_p is a multilayer perceptron (MLP) for transforming the pose latent with a rotation and translation matrix, \mathcal{D}_g^\dagger represents the network only for decoding geometry latent, and \otimes represents matrix-vector multiplication. Notice we omit frame index t and augmentation operation a for simplicity. In this way, our network is able to predict the performer's face geometry free from the disturbance of head pose variance.

We use the same triplet supervision strategy as the expression network to disentangle the face geometry and head pose, which has

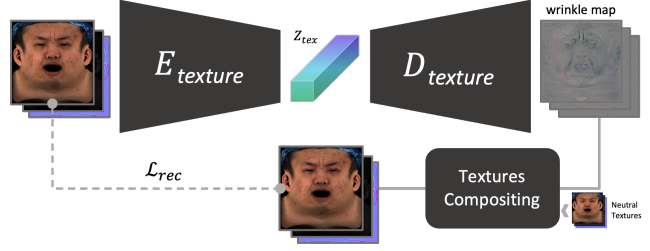


Fig. 9. **Architecture of texture network.** To enable high-resolution dynamic textures, our texture network outputs wrinkle maps instead of textures themselves. Since the textures for training are aligned in advance, our texture network only encodes textures from same frames to one latent space. We minimize the reconstruction loss after applying the predicted wrinkle maps to neutral textures.

the following metrics:

$$\begin{aligned} \mathcal{L}_{rec} &= \|G^{t,a} - \hat{G}^{t,a}\|_2 \\ \mathcal{L}_{cyc} &= \|Z_g^{t,a} - \hat{Z}_g^{t,a}\|_2 + \|Z_p^{t,a} - \hat{Z}_p^{t,a}\|_2 \\ \mathcal{L}_{geo} &= \|Z_g^{t,a} - Z_g^{s,a}\|_2 \\ \mathcal{L}_{pos} &= \|Z_p^{t,a} - Z_p^{s,a}\|_2 \\ \mathcal{L}_{cro} &= \|G^{t,a} - \tilde{G}^{t,a}\|_2 + \|G^{t,b} - \tilde{G}^{t,b}\|_2 + \|G^{s,a} - \tilde{G}^{s,a}\|_2 \end{aligned} \quad (12)$$

Where \mathcal{L}_{rec} , \mathcal{L}_{cyc} are reconstruction and cycled latent loss. \mathcal{L}_{geo} and \mathcal{L}_{pos} are distance between latents. \mathcal{L}_{cro} is the cross inference loss. The total loss for geometry network is formulated as follows:

$$\mathcal{L}_G = \mathcal{L}_{rec} + \mathcal{L}_{cyc} + \mathcal{L}_{geo} + \mathcal{L}_{pos} + \mathcal{L}_{cro}. \quad (13)$$

5.3 Learning Textures

The stabilized textures are view-independent and only contain expression information. Therefore, we build a similar VAE with only one latent space to learn representations for the three types of textures (diffuse albedo, specular intensity and normal maps) simultaneously. The network structure is illustrated in Fig. 9. Notice the captured texture is at 4K resolution, yet the output resolution of the network is typically 512, which inevitably leads to a significant loss of details. To retain the ability of rendering and editing at 4K textures, we enforce this network to predict wrinkle maps (we borrow this term from CG industry which essentially is the gradient of textures) instead of predicting the textures directly. Given an input texture T at frame t , our texture encoder E_{tex} encodes it to texture latent Z_{tex} , while our texture decoder D_{tex} predict the corresponding wrinkle maps \hat{W} from the texture latent Z_{tex} :

$$\hat{W} = \mathcal{D}_{tex}(Z_{tex}), \quad \hat{T} = \hat{W} \oplus N, \quad (14)$$

where N is the neutral texture, \hat{T} represents the reconstructed textures, and \oplus represents the adding operation. Similarly, we compute the texture reconstruction loss and cycled latent loss. During training process, the losses are formulated as:

$$\mathcal{L}_{rec} = \|T - \hat{T}\|_1, \quad \mathcal{L}_{cyc} = \|Z_{tex} - \hat{Z}_{tex}\|_2 \quad (15)$$

and the total loss for texture network is formulated as follows:

$$\mathcal{L}_T = \mathcal{L}_{rec} + \mathcal{L}_{cyc} \quad (16)$$

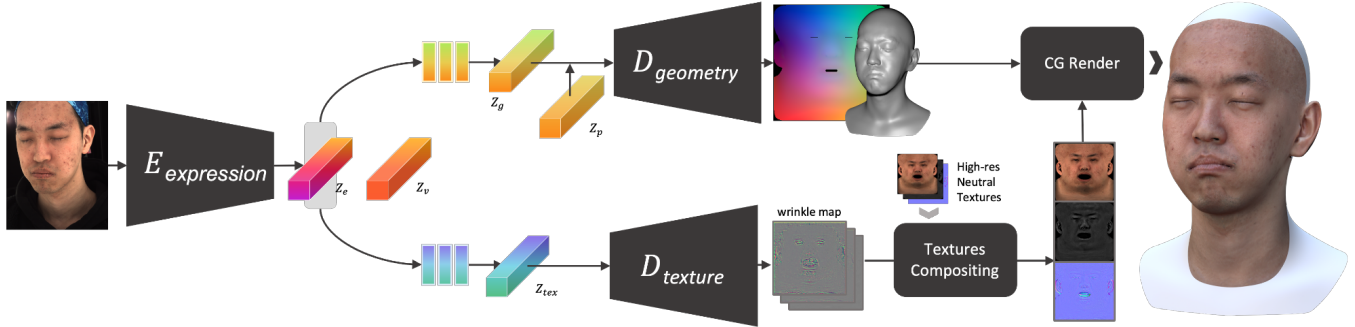


Fig. 10. **Illustration of video-driven neural physically-based face asset.** After the expression disentanglement, our method directly predicts the the realistic geometry and high-resolution textures from expression latent extracted from the input facial image. With geometry and physically-based textures, we are able to produce photo-realistic rendering result from novel view and lighting.

5.4 Unified Expression Representation

For each training frame t , our above discussed three networks predict expression latent Z_e , geometry latent Z_g and texture latent Z_{tex} respectively. Intuitively, we can learn a mapping from expressions to geometries and textures, as we have disentangled headpose and viewpoint into separate latents. We train a MLP M_e to learn mappings from facial expression latent to geometry and texture latents. Given an expression Z_e as input, M_e directly predicts \tilde{Z}_g and \tilde{Z}_{tex} as:

$$\tilde{Z}_g, \tilde{Z}_{tex} = M_e(Z_e), \quad (17)$$

The mapping loss is straightforward which minimizes the distance between encoded and mapped latents:

$$\mathcal{L}_{map} = \|Z_g - \tilde{Z}_g\|_2 + \|Z_{tex} - \tilde{Z}_{tex}\|_2. \quad (18)$$

5.5 Training and Inference

Training. Here we introduce an effective training scheme for our neural representation. We first separately train our expression, geometry and texture VAE branches (Sec. 5.1, 5.2, 5.3 respectively), to learn latent representations independently. After the three networks converge, we fix VAEs in all three branches and only train the latent mapping MLP M_e . Then, we apply an additional fine-tuning process to optimize the total loss. In this fine-tuning stage, we only lock the parameters of the expression network, and jointly train all other parts of the whole network (i.e., the geometry, texture, and mapping network). This strategy keeps the expression latent stable and allows for more precise geometry and texture adjustment by fine-tuning geometry and texture latent representations. Note that in the actual implementation, we also minimize the Kullback-Leibler (KL) divergence loss for latents in VAEs as well.

Inference. Our neural facial asset representation unifies the person specific expression, geometry and texture latents. It grants us the ability to decode geometry and physically-based texture asset directly from expressions. At the inference stage, the input is a face image with certain expressions, we then generate the expression latent using \mathcal{E}_e and use M_e to translate the encoded expression latent to geometry and texture latent. Subsequently, we use the geometry

and texture decoders \mathcal{D}_g and \mathcal{D}_{tex} to generate the face geometry, albedo, specular map and normal map. We illustrate the inference process in Fig. 10, and also formulate it as: given an input image I , we predict both geometry \tilde{G} and textures \tilde{T} with our expression encoder, latent mapping multilayer perceptron, and geometry and texture decoder:

$$\begin{aligned} Z_e &= \mathcal{E}_e(I) \\ \hat{Z}_{geo}, \hat{Z}_{tex} &= M_e(Z_e) \\ \tilde{G} &= \mathcal{D}_g(\hat{Z}_g) \\ \tilde{W} &= \mathcal{D}_{tex}(\hat{Z}_{tex}) \\ \tilde{T} &= \tilde{W} \oplus N, \end{aligned} \quad (19)$$

where the viewpoint latent and geometry pose latent are ignored, since we intend to produce results which only depend on the facial expressions of the performer. Such pipeline produces consistent geometry and textures across different views of input images due to our latent disentanglement network design.

Implementation Details. Here we describe the implementation details of our framework. The three encoders in our network have the same structure, consists of 6 sequential convolutional layers with kernel size of 5 and stride of 2 to extract latent features. Similarly, the decoders consist of 5 convolutional layers with kernel size of 3 and stride of 1 followed by pixel shuffle layers for up-sampling and residual blocks. We add a LeakyRelu layer after each convolutional layer. For further application of cross-identity neural retargeting, which will be mentioned in 6.2, inspired by Lombardi et al. [2018], we propose a similar but different network design. In our expression decoder, we concatenate a channel of zeros to each input before convolutional layers, denoted as **indicator channel**, which will be further used for cross-identity neural retargeting in 6.2.

To train the expression network, all captured face RGB images are aligned and then cropped to 256x256 before fed in as input. We precompute masks to filter out the background. The input of the geometry network is a 2D geometry image with 256x256 resolution. Aligned textures in each frame consist of a 3-channel diffuse albedo, a 3-channel normal map and a single-channel specular intensity. They are resized to 512x512 before training of the texture network.

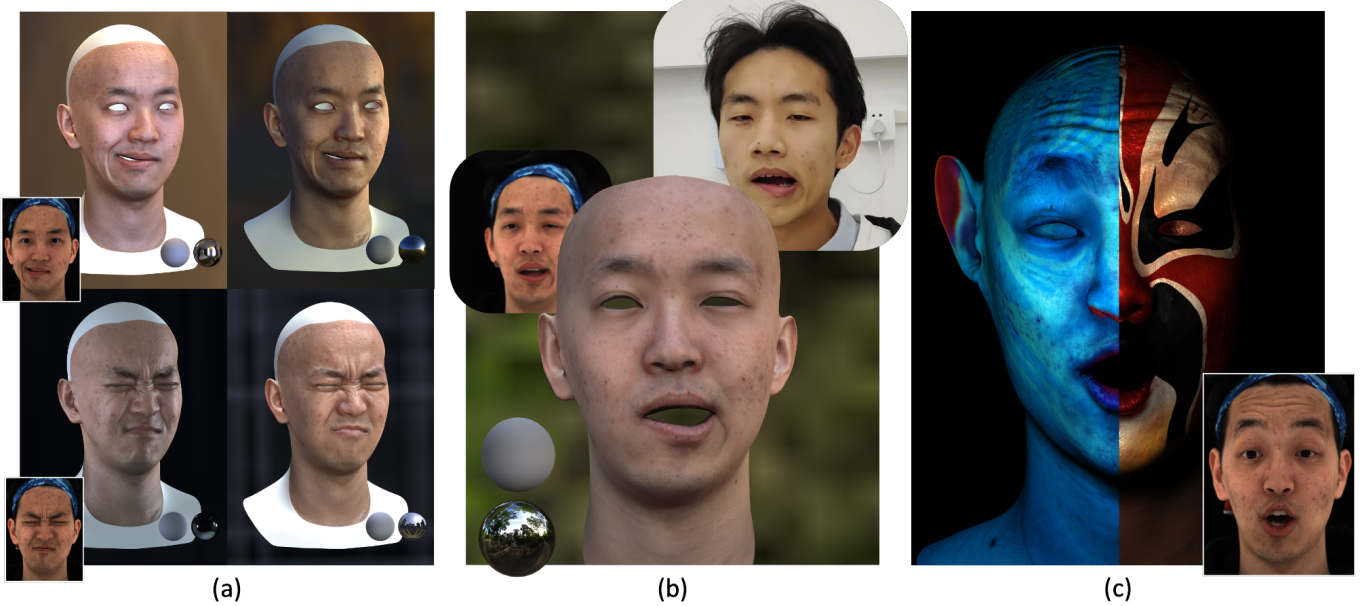


Fig. 11. Illustration of our applications. (a) performer-specific neural facial asset, (b) Cross-identity neural retargeting, (c) Geometry and texture editing.

The dimension of the expression latent, view latent and pose latent are all set to 256.

6 APPLICATIONS

Once our neural facial asset generator is trained for a specific performer, we can apply it in several production-level scenarios with minimum modification of our network. For instance, we can generalize our network to predict the performer's appearances with novel expressions or have the performer's face animated by another person's in-the-wild face video. We also introduce features including material editing, character animation and wrinkle transfer. Here we provide the implementation details of these applications, and the corresponding results are provided in the experimental section and supplementary video.

6.1 Performer-specific neural facial asset

Acquisition of per-frame geometry and physically-based textures is challenging in many ways. The capture system, like the Light Stage, generates hundreds of gigabytes of data for every second, taking days to store the data, preprocess and calculate before we can finally acquire the high-quality assets. Obtaining the assets and rendering the required footage instantly is almost impossible. With our neural facial asset generator, the expression decoder disentangles expression into latent code from the disturbance from lighting and viewpoint. During the inference stage shown in Figure 10, the neural facial asset generator takes the monocular camera footage as input and outputs the geometry as well as multi-channel wrinkle maps, which makes it possible to preview the production level dynamic facial assets instantly without complex hardware setup.

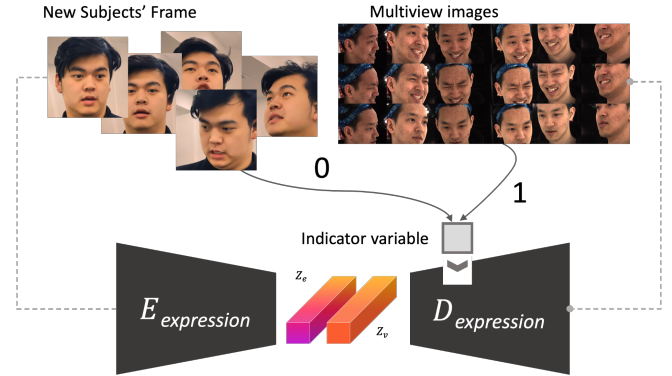


Fig. 12. Indicator variable. The indicator variable informs the decoder of which domain it should decode the image into.

6.2 Cross-identity neural retargeting

The movie and game industry always have a keen interest in facial performance capture, because of the realism it brings to the digital characters. A common request from the industry is to drive the face animation of a digital character from the facial expressions of a real performer. Recall that our expression encoder extracts the performer's expression with remarkable robustness, hence it only needs minor refinement when we apply it to another individual for expression extraction, as presented in Figure 12.

Specifically, given a well-trained neural physically-based facial asset, we apply a fine-tuning stage for the driving performer. First, we extend the expression training dataset with footage of the new subject with different expressions and varying head poses. Then, we

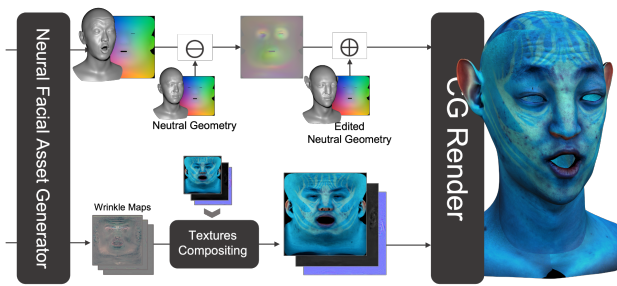


Fig. 13. **Illustration of geometry and texture editing pipeline.** Our neural facial asset generator can predict geometry deformation and wrinkle maps for an input frame. By applying the predicted deformation to the edited neutral geometry and the wrinkle maps to the edited neutral textures, we can produce the realistic appearance of a novel character with consistent expressions.

refine the expression network by training on this extended dataset. Besides the losses mentioned in Eq. 10, we simultaneously minimize the reconstruction loss of images from the new subject. To let the expression decoder reconstruct images for the driving subject, during the training process, we set the **indicator channel** of the decoder to 1 for images from footage of the driving subject and 0 for images from the original dataset. The **indicator channel** indicates whether the decoder should decode an image of the driving subject or a image of the original dataset. This indicator allows the expression latent code to contain no identity-specific information but only expressions because the decoder network can get the identity information from this indicator instead. Moreover, to ensure the encoder produces expression latent independent from identity, we further add a discriminator to supervise the latent extracted from the expression encoder. We adopt RevGrad layer proposed by Ganin and Lempitsky [2015] for the discriminator, which negates the gradient of the discriminator for the expression encoder.

Once we trained the modified expression network, we lock the parameters of it and then refine both geometry network and texture network together with the latent mapping MLP M_e on the original training dataset. Since the expression encoder extracts expression only latent, the geometry network and texture network can produce the geometry and textures from the expressions of both the original performer and the driving subject after refinement.

Then, the new subject's performance can be transferred to the original performer in the form of per-frame geometry and physically-based texture assets. Although we only take a few footages of the new subject for refinement, our neural facial asset could be driven by the new object with the same setting. The disentanglement of expression and viewpoint also allows the encoder to work stably with images taken under varying head poses, which means the new subject can even drive the performer with portable capture devices, such as cellphones and VR headsets.

6.3 Geometry and texture editing

Geometry and texture editing is important for movies and games, for example digital characters in the Avatar movie are driven by face motion capture data. Such editing require tremendous labor for artist involving novel appearances creating and then building hundreds of FACS action units and corresponding complex textures in pursuit of more realistic wrinkles.. Previous work focuses on high-precision facial capture or neural rendered final effects, yet they can not provide the artists with sufficient editability in textures, geometry, and shader to release the manual editing burden.

In contrast, with our method, driving a stylized character with edited geometry and textures become much easier, where only the neutral geometry and textures for the fictional character are needed. The editing effort can be significantly reduced, as presented in Figure 13.

To drive the stylized character, we first create the character under neutral expression that is slightly different, with artificial facial details and novel skin appearances. We can modify the geometry to change facial features, e.g. longer ears and thinner cheeks. Similarly, we can modify the textures by painting on diffuse albedo, changing micro-geometry on normal map and editing specular intensity. We expect this new character to exhibit similar movements in facial muscle and wrinkle details. Then, we transfer the dynamic facial geometry as well as wrinkle maps under different expressions to achieve realistic driving result on this new character.

Taking the driving subject's facial performance video as input, our neural facial asset can predict per-frame dynamic geometry. We regard the facial movement as offset field, which could be easily applied to other face geometry for exhibiting the same expression. We calculate the offset of our predicted geometry map with regard to the neutral geometry map of the facial asset, and then apply the offset to the neutral geometry map of stylized character to obtain the geometry with the same expression.

Our facial asset predicts wrinkle maps for textures as well. During the texture compositing stage, we replace the original neutral textures with an exquisitely drawn one. Because our network is designed to predict wrinkle maps, it can generate realistic textures under arbitrary appearance. The multi-channel wrinkle maps for each input video frame can transfer the performer's wrinkles to the stylized character realistically.

7 RESULTS

In this section, we demonstrate the capability of our approach on a variety of scenarios. We first report the implementation details of our approach and the dataset captured by our FaStage, and then analyze our results in various editing scenarios. We further provide a comparison with previous methods and evaluations of our main technical components, both qualitatively and quantitatively. The limitation and discussions regarding our approach are provided in the last subsection.

Dataset and Implementation Details. To train and evaluate our method, we capture a dynamic facial asset dataset with physically-based textures using our FaStage system. Our capture system is



Fig. 14. Our results of Neural Physically-based Facial Assets.

shown in Fig. 4, where all the cameras are calibrated and synchronized with lighting in advance. During capture, the machine vision camera array produces 27 RGB streams at 2592×2048 resolution, while the high-speed camera array generates 3 RGB streams at 4096×2304 resolution. After data pre-processing, we produce 4096×4096 unwrapped physically-based textures for each frame, including diffuse albedo, normal map, and specular intensity. Our dataset consists of three performers and for each performer, we capture a total number of 7200 frames. We run all of our experiments with a single Nvidia A6000 GPU. Additionally, we adopt Blender’s Eevee as our main render engine as it is free, open-source, fast and convenient. Rendering a frame with textures of 4k resolution takes around 2.0 seconds with Eevee engine. We further utilize the rendering shader provided in the Heretic [Technologies 2020] to achieve real-time performance. Fig. 14 demonstrates several neural facial assets generated using our approach, which enables highly realistic facial capture and physically-based editing.

7.1 Video-driven Applications on Novel Expressions

Our multi-VAE based neural facial assets enable various video-driven applications, ranging from fine-grained facial capture, to cross-identity facial motion retargeting, and to geometry and physically-based texture editing. As shown in Fig. 15, our approach enables high-quality dynamic facial geometry generation with pore-level dynamic physically-based textures on complicated expressions of the specific performer, such as frowning or winking. Such video-driven results can be integrated into existing physically-based render to generate highly realistic rendering with the facial idiosyncrasies of the performer for production. Fig. 16 further provides the video-driven results using the RGB footage of different performers. Thanks to our fast data-driven adaptation within the multi-VAE framework, our approach enables highly-fidelity and automatic cross-identity facial motion retargeting, without the extra requirement for tedious manual labor, various facial rigs or temporally-aligned pair-wise

samples. Besides, our physically-based retargeted animations are temporally consistent, which is provided in the accompanying video. In general, our

In addition to driving the captured performer, our method further enables convenient physically-based editing for generating and driving an artistically stylized avatar. To build a stylized avatar, the geometry of the neutral expression is stylized to obtain novel physiognomy, such as longer ears and thinner cheeks. Then, the neutral textures can also be edited and stylized according to the appearance of the new avatar. Our approach can faithfully predict wrinkle maps on novel expressions, which can be applied to the edited neutral geometry and texture, so as to generate highly realistic dynamic stylized characters whilst still maintaining the identity of the captured performer. Fig. 17 shows the photo-realistic rendering results of our artistically stylized video-driven facial assets. We transfer the performers into various stylized characters, such as Guan Yu the most famous red-face character in traditional Chinese Peking Opera for Three Kingdoms, and the impressive blue alien from the feature film AVATAR. We can also edit or paint the performer’s neutral asset to enable video-driven VFX results, such as paint a realistic mental Deemos logo on the cheek, add realistic face painting or adjust the facial roughness to generate more shiny skin. These fancy results in Fig. 17 demonstrate the effectiveness and convenience of our approach for realistic dynamic facial editing.

7.2 Comparisons

To the best of our knowledge, our approach is the first to provide video-driven facial geometries with dynamic physically-based texture assets. To demonstrate the video-driven performance of our approach, we compare against various video-driven facial reconstruction and animation methods, including parametric facial model DECA proposed by Feng et al. [2021], a performer-specific method for production proposed by Laine et al. [2017], and Deep Appearance Model proposed by Lombardi et al. [2018]. We adopt the official

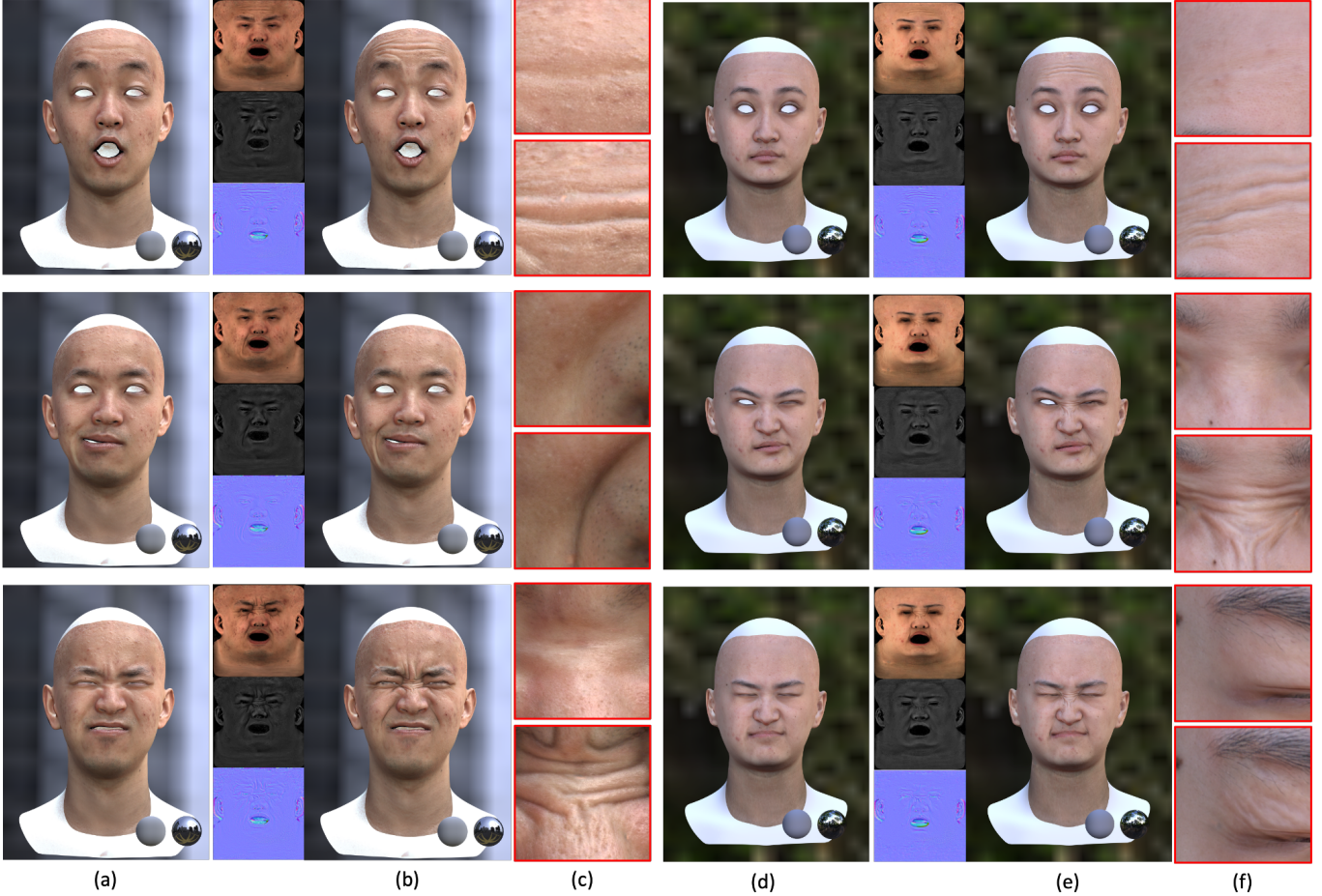


Fig. 15. **Video-driven Neural Physically-based Facial Asset.** Our dynamic textures effectively enhance the appearance of the performer: (a,d) driven facial assets with only static neutral physically-based textures, (b,e) driven facial assets with dynamic physically-based textures, (c,f) zoom-in view. Our method successfully models the dynamic textures and preserves facial details at high resolution.

pre-trained PyTorch model for the method of Feng et al. [2021], and faithfully re-implement both the methods of Laine et al. [2017] and Lombardi et al. [2018] and train their models using the same training dataset as ours for a fair comparison. Due to the lack of available code of the method of Moser et al. [2021], we only compare the statistic results against several methods, including the one of Moser et al. [2021], which demonstrates our approach achieves more comprehensive capabilities to reconstruct various facial attributes.

Fig. 18 provides the qualitative comparison on our testing dataset for the task of facial geometry capture from in-the-wild monocular video input. It is worth noting that compared to other methods, our approach generates more realistic pore-level facial details which are exhibited in normal maps. Besides, both the methods of Laine et al. [2017] and Lombardi et al. [2018] suffer from poor facial capture performance when handling side-view input. In contrast, our approach generates more realistic video-driven facial animation results even under challenging expressions, which compares favorably to other methods. For fair quantitative comparison, we first transform the

Capability	2017	2018	2021	Ours
Animateable geometry	✓	✓	✓	✓
Retargeting		✓	✓	✓
Dynamic textures		✓		✓
Relightable textures		✓		✓
Editable material				✓
Transferable wrinkle				✓

Table 1. **Comparison of capability against the state-of-the-art methods.** We compare our method against the methods of Laine et al. [2017], Lombardi et al. [2018] and Moser et al. [2021].

output models on our testing dataset from both Laine et al. [2017] and Lombardi et al. [2018] into our geometry map representation. Note that the coordinates of geometries are centered and normalized to $[-1, 1]$ and we adopt RMSE as the metric. As shown in Fig. 19 and Tab. 2, our approach consistently outperforms the baselines,

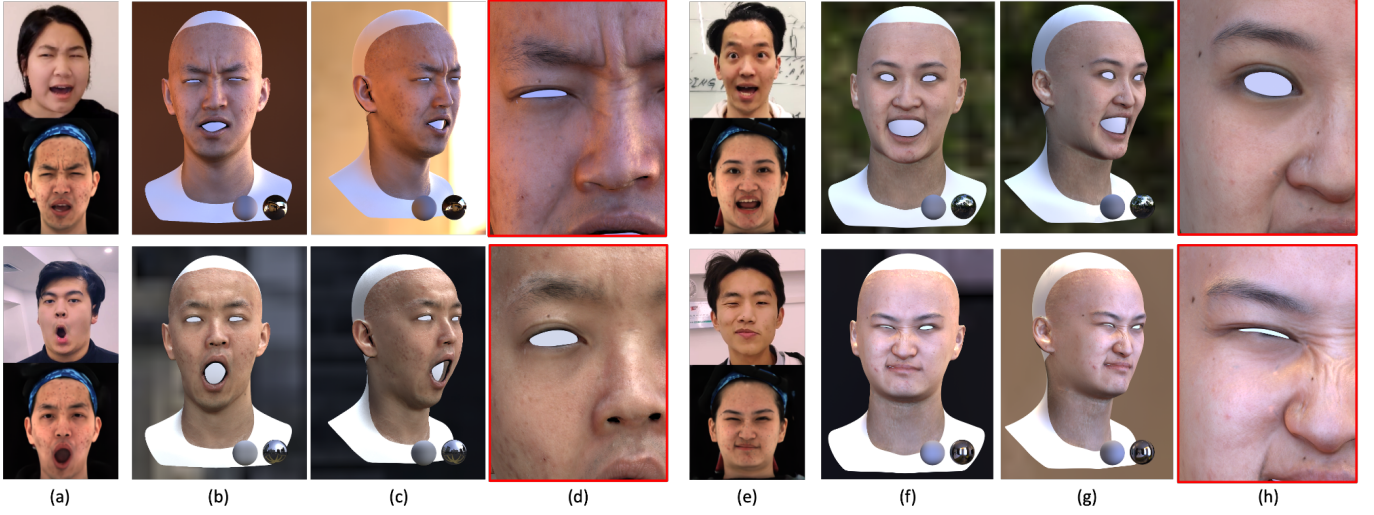


Fig. 16. **Cross-identity video driven results.** We extend the expression network for new subjects with different expressions and varying head poses: (a,e) the upper image is the new performer’s expression, and the lower image is the neural retargeting results from our expression decoder, (b,f) driven facial asset in front view, (c,g) driven facial asset in the left view, (d,h) zoom-in view. Our method achieves detailed video-driven results from different identities with dynamic textures, which leads to photo-realistic rendering.

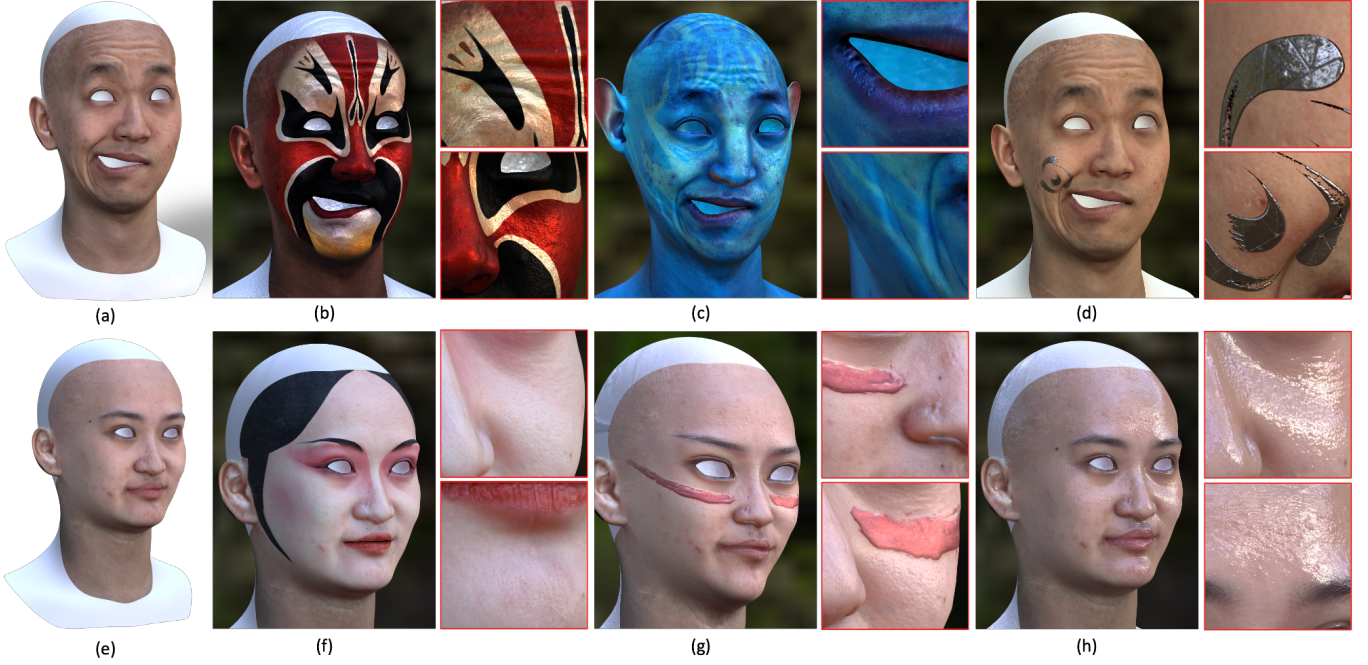


Fig. 17. **Geometry and texture editing results.** We edit the video-driven facial assets (a,e) in various ways: (b) We paint the diffuse albedo with the style of Guan Yu, the most famous red-face character in traditional Chinese Peking Opera; (c) We stylize the geometry of the performer to the blue alien from the feature film AVATAR with a novel facial structure but consistent identity features; (d) We add a metal Deemos logo to the cheek of the performer by modifying the textures; (f) We paint the diffuse albedo with the style of Yu Ji, the beloved concubine of Xiang Yu, the hegemon of Western Chu, from the famous Peking Opera *Farewell My Concubine*; (g) We altered the performer’s facial structure, and added realistic face painting by jointly modifying the diffuse albedo and the normal map; (g) We adjust the facial roughness to give the skin a more shiny look.

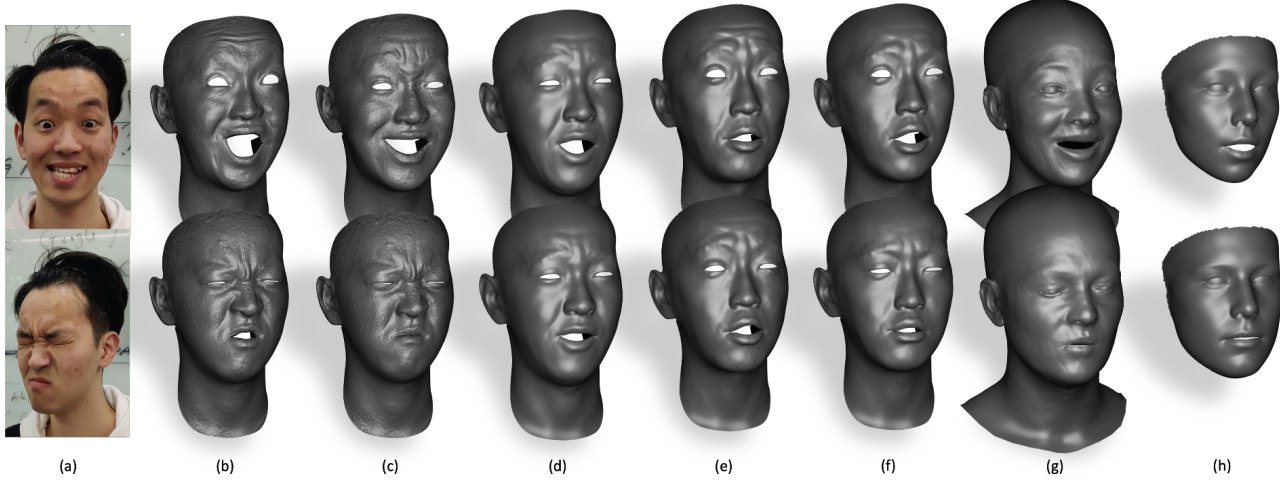


Fig. 18. **Qualitative comparison of video-driven result on in-the-wild monocular RGB inputs.** (a) the input in-the-wild image, (b) predicted geometry of our method with normal map, before the refinement using in-the-wild images, (c) predicted geometry of our method with normal map, after the refinement using in-the-wild images, (d) predicted geometry of Laine et al. [2017], (e) predicted geometry of Lombardi et al. [2018], before the refinement using in-the-wild images, (f) predicted geometry of Lombardi et al. [2018], after the refinement using in-the-wild images, (g) predicted geometry of Feng et al. [2021], (h) predicted geometry of Guo et al. [2020]. With a quick refinement, our method can deal with head pose and lighting variance better than other methods.

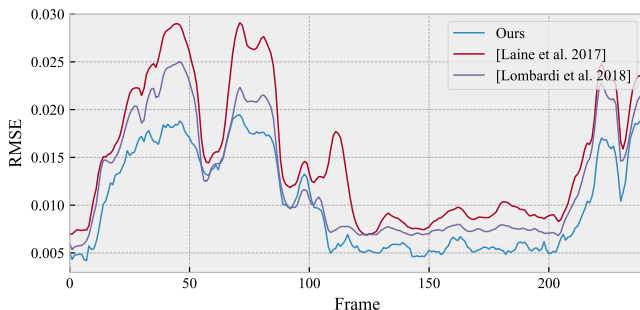


Fig. 19. **Quantitative comparison against several state-of-the-art methods.** We compare the per-frame geometric reconstruction errors on an image sequence in our testing dataset. Our method stays accurate throughout testing.

which demonstrates the superiority of our approach for dynamic video-driven facial capture and modeling.

7.3 Ablation Study

Here, we evaluate the performance of different training strategies and demonstrate the effectiveness of our multi-VAE network designs. Specifically, we evaluate the expression disentanglement, the pose enhancement and wrinkle-based texture prediction in our express, geometry and texture VAE, respectively.

Expression disentanglement. We compare the performance of our model with or without the expression disentanglement training

Method	RMSE
[Laine et al. 2017]	0.015061
[Lombardi et al. 2018]	0.012564
Ours	0.010205

Table 2. **Quantitative comparison against state-of-the-art methods.** We compare the overall geometric reconstruction errors on the images from our testing dataset. Our method outperforms others, indicating the better expression ability of our network.

scheme. Let **w/o disentanglement** denote the variation of our approach without triplet input for both expression and geometry VAEs. We utilize the same use multi-view images as input for training, but ignore the viewpoint information. During the training process of expression network, we only adopt the loss \mathcal{L}_{rec} in Eq. 6, and remove viewpoint latent from our network. As shown in Fig. 20, our scheme with expression disentanglement enables more accurate and consistent prediction for geometry, especially when the input viewpoint changes. Our expression disentanglement training scheme facilitates the robustness of our model to handle viewpoint variance.

Pose extraction. Here we compare against our variation without encoding the pose latent from geometry while keeping the input geometry intact without augmentation, denoted as **w/o pose**. During the training process, we only adopt the first two loss items in Eq. 13. As illustrated in Fig. 21, the results of **w/o pose** are temporally unstable. We observe several sudden changes in geometry, leading to the spikes of the curves in Fig. 21. Such unstable phenomenon

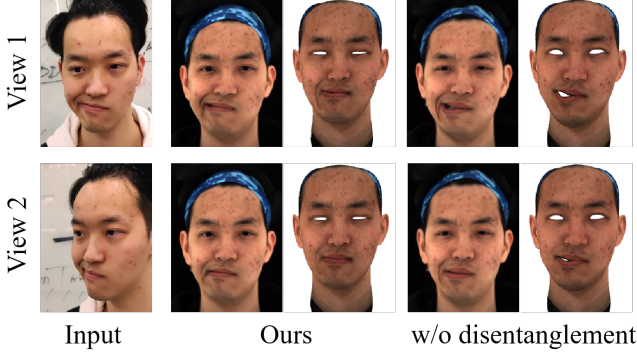


Fig. 20. Qualitative evaluation of our expression disentanglement. After training the network with the same dataset, we tested it with images from novel viewpoints. The variation without expression disentanglement suffers from inconsistency when the viewpoint changes. The absence of expression and viewpoint disentanglement leads to a reduced ability of generalization for our model. As a comparison, the results given by our model with expression disentanglement training handled viewpoint change with no deterioration in performance.

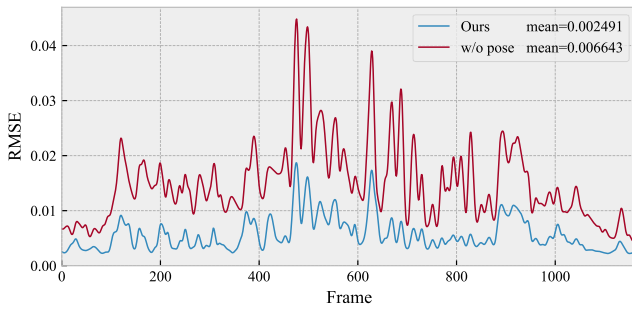


Fig. 21. Quantitative evaluation of our pose augmentation. We evaluate the stability of the predicted geometries with and without pose augmentations. The curve shows the mean distances of vertices to their stable coordinates, which are expected to be fixed. Our training scheme with pose augmentation leads to more stable face geometries, while the results given by the variation without it jitters while testing.

largely compromises the performance of facial animation, causing tedious manual correction for post-production. Differently, our pose enhancement handle the head pose variance, so as to alleviate the unstable artifact.

Texture prediction strategy. We further evaluate our wrinkle-map-based texture prediction strategy. Let **w/o wrinkle** denote our variation that directly predicts pixel-aligned textures instead of wrinkle maps and subsequently adopts an extra super-resolution network upscale the predicted textures to 4K resolution. As shown in Fig. 22, our scheme models the wrinkle maps including shading maps, which enables better preservation of facial details. Our wrinkle map models the discrepancies on top of the neutral textures and can be scale to high-resolution without suffering from blur or block-wise artifacts.

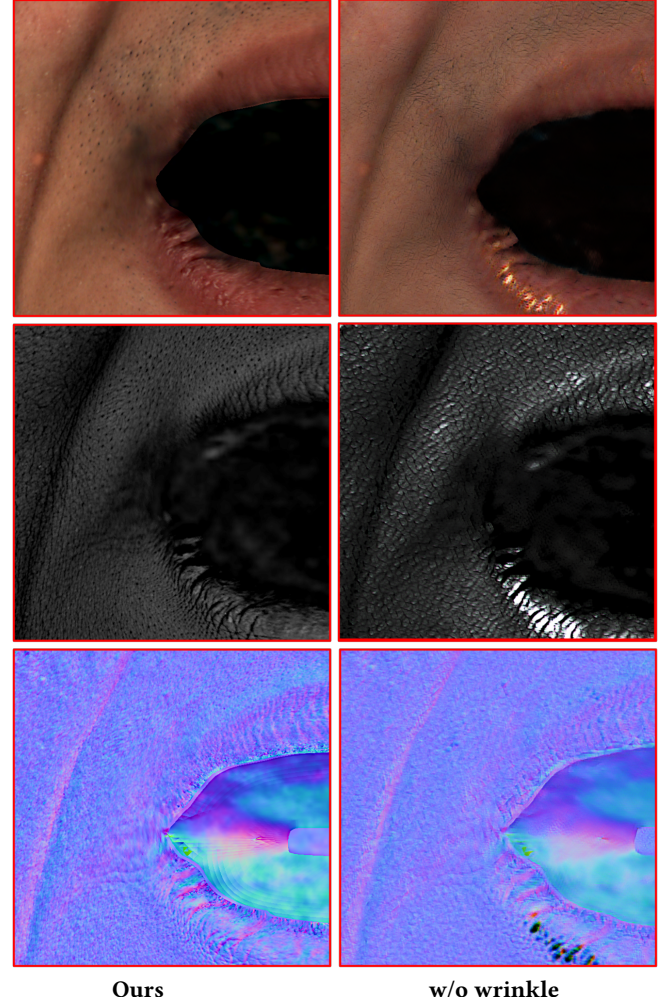


Fig. 22. Qualitative evaluation of our texture predicting strategy. Our variation without predicting wrinkles suffers from repeated artifacts and loses a lot of real details. The wrinkle map preserves more facial details and sharpens the textures. scale-like artifact.

7.4 Limitations and Discussions

We have demonstrated the compelling capability of our method in a variety of applications with production-level rendering results. Nevertheless, our approach is subject to several limitations.

The performance of our method relies heavily on the quality of the training data. However, our FaStage is extremely expensive to build and the data collection and pre-processing are time-consuming, preventing our approach from daily usage for everybody. We will further explore the possibility of capturing training data with light-weight equipment and improving our data processing efficiency while maintaining the performance of our method.

Within the performer-specific paradigm, our method can not handle extremely challenging identity and environmental variance. Our model achieved cross-identity facial performance retargeting

with robust expression disentanglement, yet the application environment, such as lighting conditions and background, was not well simulated as previous papers (i.e. Klaudiny et al. [2017]) focused on face capture did. Although our expression network inherently handles cross-identity input, we did not embed neural redirection structures into it, which restricts the performance of our method for multi-identity tasks. In future works, we will apply portrait matting and single image relighting techniques (i.e. Zhang et al. [2021]) as a way to simulate novel lighting environments. We will also design a new training pipeline for multi-identity tasks.

We still need other facial components to improve the authenticity of our facial assets. Our geometry network only modeled the movements of the face, but not that of other facial components like teeth, gums, eyeballs, lacrimal fluid, eye occlusion, and eyelashes. Previous work applied different types of deformation such as linear deformation and laplacian deformation to model the movements for these components. However, these types of deformation may not be realistic enough, especially when modeling eye movements. In future works, we will incorporate eye movement capture and jaw adaptation algorithms into our model, and use a biologically sound parametric skull model as prior. Apart from other facial components, we also need photo-realistic hair to build a high-quality digital avatar. Rendering hair remains a challenging problem in computer graphics due to the hair’s complex physical properties. Existing solutions are mostly computationally expensive, yet recent works on neural radiance field [Mildenhall et al. 2020] have shown promising results in the task of rendering fuzzy objects. We will further improve our method by adding hair to our render results with the method of [Luo et al. 2021].

We disentangle the textures into neutral textures and multi-channel wrinkle maps. Despite the fact that we can use them to modify high-resolution textures, they can not simulate the phenomena of pore squeezing. A possible solution is applying a similar strategy like the one we use at the data processing stage, where we disentangle the textures into warp fields and neutral textures to eliminate the pixel drift. It has the ability to model skin stretch and compression, but we can not use this technique when we generate textures due to the jittering output resulting from excessive data noise. In future works, we will further enhance our data processing capabilities, which will allow us to upgrade our wrinkle-map-based texture inference method to a warp-field-based one. In this way, the dynamic textures given by our network will be able to simulate pore-level extrusion.

8 CONCLUSION

We have presented a neural approach to generate video-driven dynamic facial geometries with high-quality physically-based texture assets for production from FaStage data. Our neural approach enables high-fidelity performer-specific facial capture and even cross-identity facial motion retargeting without tedious manual labor. It also enables various high-realistic, convenient and physically-based facial editing effects, like geometry and material editing or wrinkle transfer. The core of our approach is a new multi-VAE based design to disentangle facial attributes explicitly and effectively with the aid of a global MLP-based mapping across latent spaces. Our explicit expression and viewpoint disentanglement as well as a novel triplet

semi-supervision scheme enable effective latent space construction for both the expression and geometry VAEs. Our wrinkle maps and view-independent texture inference in our physically-based texture VAE achieve high-quality 4K rendering of dynamic textures and convenient neutral-based editing for post-production. Our multi-stage training framework for all the facial attributes enables effective generation of our neural assets. We demonstrate extensive experimental results and video-driven applications for production-level facial animation, facial motion retargeting and physically-based editing with high realism. We believe that our approach renews the video-driven production-level workflows of generating dynamic facial geometries with physically-based assets in the neural era. It serves as a critical step for automatic, high-quality and controllable dynamic facial asset generation, with many potential applications for believable digital human, film and game production and immersive experience in VR/AR and Metaverse.

REFERENCES

Victoria Fernández Abrevaya, Adnane Boukhayma, Philip HS Torr, and Edmond Boyer. 2020. Cross-modal deep face normals with deactivable skip connections. In *Proceedings of the IEEE/CVF Conference on Computer Vision and Pattern Recognition*. 4979–4989.

Linchao Bao, Xiangkai Lin, Yajing Chen, Haoxian Zhang, Sheng Wang, Xuefei Zhe, Di Kang, Haozhi Huang, Xinwei Jiang, Jue Wang, et al. 2021. High-Fidelity 3D Digital Human Head Creation from RGB-D Selfies. *ACM Transactions on Graphics (TOG)* 41, 1 (2021), 1–21.

Thabo Beeler, Bernd Bickel, Paul Beardsley, Bob Sumner, and Markus Gross. 2010. High-quality single-shot capture of facial geometry. In *ACM SIGGRAPH 2010 papers*. 1–9.

Sai Bi, Stephen Lombardi, Shunsuke Saito, Tomas Simon, Shih-En Wei, Kevyn Mcphail, Ravi Ramamoorthi, Yaser Sheikh, and Jason Saragih. 2021. Deep relightable appearance models for animatable faces. *ACM Transactions on Graphics (TOG)* 40, 4 (2021), 1–15.

Volker Blanz and Thomas Vetter. 1999. A morphable model for the synthesis of 3D faces. In *Proceedings of the 26th annual conference on Computer graphics and interactive techniques*. 187–194.

Egor Burkov, Igor Paschenk, Artur Grigorev, and Victor Lempitsky. 2020. Neural head reenactment with latent pose descriptors. In *Proceedings of the IEEE/CVF Conference on Computer Vision and Pattern Recognition*. 13786–13795.

Chen Cao, Vasu Agrawal, Fernando De La Torre, Lele Chen, Jason Saragih, Tomas Simon, and Yaser Sheikh. 2021. Real-time 3D neural facial animation from binocular video. *ACM Transactions on Graphics (TOG)* 40, 4 (2021), 1–17.

Chen Cao, Derek Bradley, Kun Zhou, and Thabo Beeler. 2015. Real-time high-fidelity facial performance capture. *ACM Transactions on Graphics (TOG)* 34, 4 (2015), 1–9.

Chen Cao, Yanlin Weng, Stephen Lin, and Kun Zhou. 2013. 3D shape regression for real-time facial animation. *ACM Transactions on Graphics (TOG)* 32, 4 (2013), 1–10.

Chen Cao, Yanlin Weng, Shun Zhou, Yiyi Tong, and Kun Zhou. 2014. FaceWarehouse: A 3D Facial Expression Database for Visual Computing. *IEEE Transactions on Visualization and Computer Graphics* 20, 3 (2014), 413–425. <https://doi.org/10.1109/TVCG.2013.249>

Anpei Chen, Zhang Chen, Guli Zhang, Kenny Mitchell, and Jingyi Yu. 2019. Photo-realistic facial details synthesis from single image. In *Proceedings of the IEEE/CVF International Conference on Computer Vision*. 9429–9439.

Lele Chen, Chen Cao, Fernando De la Torre, Jason Saragih, Chenliang Xu, and Yaser Sheikh. 2021. High-fidelity Face Tracking for AR/VR via Deep Lighting Adaptation. In *Proceedings of the IEEE/CVF Conference on Computer Vision and Pattern Recognition*. 13059–13069.

Paul Debevec, Tim Hawkins, Chris Tchou, Haarm-Pieter Duiker, Westley Sarokin, and Mark Sagar. 2000. Acquiring the reflectance field of a human face. In *Proceedings of the 27th annual conference on Computer graphics and interactive techniques*. 145–156.

Bernhard Egger, William AP Smith, Ayush Tewari, Stefanie Wuhrer, Michael Zollhoefer, Thabo Beeler, Florian Bernard, Timo Bolkart, Adam Kortylewski, Sami Romdhani, et al. 2020. 3d morphable face models—past, present, and future. *ACM Transactions on Graphics (TOG)* 39, 5 (2020), 1–38.

Paul Ekman and Wallace V Friesen. 1978. Facial action coding system. *Environmental Psychology & Nonverbal Behavior* (1978).

Yao Feng, Haiwen Feng, Michael J. Black, and Timo Bolkart. 2021. Learning an Animatable Detailed 3D Face Model from In-The-Wild Images. *ACM Transactions on Graphics (Proc. SIGGRAPH)* 40, 8. <https://doi.org/10.1145/3450626.3459936>

Yao Feng, Fan Wu, Xiaohu Shao, Yanfeng Wang, and Xi Zhou. 2018. Joint 3d face reconstruction and dense alignment with position map regression network. In *Proceedings of the European Conference on Computer Vision (ECCV)*. 534–551.

Graham Fyffe and Paul Debevec. 2015. Single-shot reflectance measurement from polarized color gradient illumination. In *2015 IEEE International Conference on Computational Photography (ICCP)*. IEEE, 1–10.

Graham Fyffe, Tim Hawkins, Chris Watts, Wan-Chun Ma, and Paul Debevec. 2011. Comprehensive facial performance capture. In *Computer Graphics Forum*, Vol. 30. Wiley Online Library, 425–434.

Guy Gafni, Justus Thies, Michael Zollhofer, and Matthias Nießner. 2021. Dynamic neural radiance fields for monocular 4d facial avatar reconstruction. In *Proceedings of the IEEE/CVF Conference on Computer Vision and Pattern Recognition*. 8649–8658.

Yaroslav Ganin and Victor Lempitsky. 2015. Unsupervised Domain Adaptation by Backpropagation. In *Proceedings of the 32nd International Conference on Machine Learning (Proceedings of Machine Learning Research, Vol. 37)*. Francis Bach and David Blei (Eds.). PMLR, Lille, France, 1180–1189. <https://proceedings.mlr.press/v37/ganin15.html>

Baris Gecer, Stylianos Ploumpis, Irene Kotsia, and Stefanos Zafeiriou. 2019. Ganfit: Generative adversarial network fitting for high fidelity 3d face reconstruction. In *Proceedings of the IEEE/CVF Conference on Computer Vision and Pattern Recognition*. 1155–1164.

Abhijeet Ghosh, Graham Fyffe, Borom Tunwattanapong, Jay Busch, Xueming Yu, and Paul Debevec. 2011. Multiview face capture using polarized spherical gradient illumination. In *Proceedings of the 2011 SIGGRAPH Asia Conference*. 1–10.

Paulo Gotardo, Jérémie Rivière, Derek Bradley, Abhijeet Ghosh, and Thabo Beeler. 2018. Practical dynamic facial appearance modeling and acquisition. (2018).

Jianzhu Guo, Xiangyu Zhu, Yang Yang, Fan Yang, Zhen Lei, and Stan Z Li. 2020. Towards Fast, Accurate and Stable 3D Dense Face Alignment. In *Proceedings of the European Conference on Computer Vision (ECCV)*.

Kaiwen Guo, Peter Lincoln, Philip Davidson, Jay Busch, Xueming Yu, Matt Whalen, Geoff Harvey, Sergio Orts-Escalona, Rohit Pandey, Jason Dourgarian, et al. 2019. The relightables: Volumetric performance capture of humans with realistic relighting. *ACM Transactions on Graphics (TOG)* 38, 6 (2019), 1–19.

Yudong Guo, Jianfei Cai, Boyi Jiang, Jianmin Zheng, et al. 2018. Cnn-based real-time dense face reconstruction with inverse-rendered photo-realistic face images. *IEEE transactions on pattern analysis and machine intelligence* 41, 6 (2018), 1294–1307.

Loc Huynh, Weikai Chen, Shunsuke Saito, Jun Xing, Koki Nagano, Andrew Jones, Paul Debevec, and Hao Li. 2018. Mesoscopic facial geometry inference using deep neural networks. In *Proceedings of the IEEE Conference on Computer Vision and Pattern Recognition*. 8407–8416.

Hanbyul Joo, Tomas Simon, Xulong Li, Hao Liu, Lei Tan, Lin Gui, Sean Banerjee, Timothy Scott Godisart, Bart Nabbe, Iain Matthews, Takeo Kanade, Shohei Nobuhara, and Yaser Sheikh. 2017. Panoptic Studio: A Massively Multiview System for Social Interaction Capture. *IEEE Transactions on Pattern Analysis and Machine Intelligence* (2017).

Davis E King. 2009. Dlib-ml: A machine learning toolkit. *The Journal of Machine Learning Research* 10 (2009), 1755–1758.

Diederik P. Kingma and Max Welling. 2014. Auto-Encoding Variational Bayes. In *2nd International Conference on Learning Representations, ICLR 2014, Banff, AB, Canada, April 14–16, 2014, Conference Track Proceedings*. arXiv:<http://arxiv.org/abs/1312.6114v10> [stat.ML]

Martin Klaudiny, Steven McDonagh, Derek Bradley, Thabo Beeler, and Kenny Mitchell. 2017. Real-Time Multi-View Facial Capture with Synthetic Training. In *Computer Graphics Forum*, Vol. 36. Wiley Online Library, 325–336.

Samuli Laine, Tero Karras, Timo Aila, Antti Hervä, Shunsuke Saito, Ronald Yu, Hao Li, and Jaakko Lehtinen. 2017. Production-level facial performance capture using deep convolutional neural networks. In *Proceedings of the ACM SIGGRAPH/Eurographics symposium on computer animation*. 1–10.

Alexandros Lattas, Stylianos Moschoglou, Stylianos Ploumpis, Baris Gecer, Abhijeet Ghosh, and Stefanos P Zafeiriou. 2021. AvatarMe++: Facial Shape and BRDF Inference with Photorealistic Rendering-Aware GANs. *IEEE Transactions on Pattern Analysis & Machine Intelligence* 01 (2021), 1–1.

Chloe LeGendre, Kalle Bladin, Bipin Kishore, Xinglei Ren, Xueming Yu, and Paul Debevec. 2018. Efficient multispectral facial capture with monochrome cameras. In *Color and Imaging Conference*, Vol. 2018. Society for Imaging Science and Technology, 187–202.

John P Lewis, Ken Anjyo, Taehyun Rhee, Mengjie Zhang, Frederic H Pighin, and Zhiqiang Deng. 2014. Practice and Theory of Blendshape Facial Models. *Eurographics (State of the Art Reports)* 1, 8 (2014), 2.

Jiaman Li, Zhengfei Kuang, Yajie Zhao, Mingming He, Karl Bladin, and Hao Li. 2020b. Dynamic facial asset and rig generation from a single scan. *ACM Trans. Graph.* 39, 6 (2020), 215–1.

Ruiling Li, Karl Bladin, Yajie Zhao, Chinmay Chinara, Owen Ingraham, Pengda Xiang, Xinglei Ren, Pratusha Prasad, Bipin Kishore, Jun Xing, et al. 2020a. Learning formation of physically-based face attributes. In *Proceedings of the IEEE/CVF Conference on Computer Vision and Pattern Recognition*. 3410–3419.

Tianye Li, Tim Bolkart, Michael J. Black, Hao Li, and Javier Romero. 2017. Learning a model of facial shape and expression from 4D scans. *ACM Transactions on Graphics (Proc. SIGGRAPH Asia)* 36, 6 (2017), 194:1–194:17. <https://doi.org/10.1145/3130800.3130813>

Stephen Lombardi, Jason Saragih, Tomas Simon, and Yaser Sheikh. 2018. Deep appearance models for face rendering. *ACM Transactions on Graphics (TOG)* 37, 4 (2018), 1–13.

Stephen Lombardi, Tomas Simon, Jason Saragih, Gabriel Schwartz, Andreas Lehrmann, and Yaser Sheikh. 2019. Neural Volumes: Learning Dynamic Renderable Volumes from Images. *ACM Trans. Graph.* 38, 4, Article 65 (July 2019), 14 pages.

Stephen Lombardi, Tomas Simon, Gabriel Schwartz, Michael Zollhofer, Yaser Sheikh, and Jason Saragih. 2021. Mixture of Volumetric Primitives for Efficient Neural Rendering. *ACM Trans. Graph.* 40, 4, Article 59 (jul 2021), 13 pages. <https://doi.org/10.1145/3450626.3459863>

Matthew Loper, Naureen Mahmood, Javier Romero, Gerard Pons-Moll, and Michael J. Black. 2015. SMPL: A Skinned Multi-Person Linear Model. *ACM Trans. Graphics (Proc. SIGGRAPH Asia)* 34, 6 (Oct. 2015), 248:1–248:16.

Haimin Luo, Anpei Chen, Qixuan Zhang, Bai Pang, Minye Wu, Lan Xu, and Jingyi Yu. 2021. Convolutional Neural Opacity Radiance Fields. *arXiv preprint arXiv:2104.01772* (2021).

Shugao Ma, Tomas Simon, Jason Saragih, Dawei Wang, Yuecheng Li, Fernando De La Torre, and Yaser Sheikh. 2021. Pixel Codec Avatars. In *Proceedings of the IEEE/CVF Conference on Computer Vision and Pattern Recognition*. 64–73.

Wan-Chun Ma, Tim Hawkins, Pieter Peers, Charles-Felix Chabert, Malte Weiss, Paul E Debevec, et al. 2007. Rapid Acquisition of Specular and Diffuse Normal Maps from Polarized Spherical Gradient Illumination. *Rendering Techniques* 2007, 9 (2007), 10.

Ben Mildenhall, Pratul P Srinivasan, Matthew Tancik, Jonathan T Barron, Ravi Ramamoorthi, and Ren Ng. 2020. Nerf: Representing scenes as neural radiance fields for view synthesis. In *European conference on computer vision*. Springer, 405–421.

Araceli Morales, Gemma Piella, and Federico M Sukno. 2021. Survey on 3D face reconstruction from uncalibrated images. *Computer Science Review* 40 (2021), 100400.

Lucio Moser, Chinyu Chien, Mark Williams, Jose Serra, Darren Hendler, and Doug Roble. 2021. Semi-supervised video-driven facial animation transfer for production. *ACM Transactions on Graphics (TOG)* 40, 6 (2021), 1–18.

Yuval Nirkin, Yosi Keller, and Tal Hassner. 2019. Fsgan: Subject agnostic face swapping and reenactment. In *Proceedings of the IEEE/CVF international conference on computer vision*. 7184–7193.

Kyle Olszewski, Joseph J Lim, Shunsuke Saito, and Hao Li. 2016. High-fidelity facial and speech animation for VR HMDs. *ACM Transactions on Graphics (TOG)* 35, 6 (2016), 1–14.

Pascal Paysan, Reinhard Knothe, Brian Amberg, Sami Romdhani, and Thomas Vetter. 2009. A 3D face model for pose and illumination invariant face recognition. In *2009 sixth IEEE international conference on advanced video and signal based surveillance*. Ieee, 296–301.

Amit Raj, Michael Zollhofer, Tomas Simon, Jason Saragih, Shunsuke Saito, James Hays, and Stephen Lombardi. 2021. Pixel-Aligned Volumetric Avatars. In *Proceedings of the IEEE/CVF Conference on Computer Vision and Pattern Recognition*. 11733–11742.

Elad Richardson, Matan Sela, and Ron Kimmel. 2016. 3D face reconstruction by learning from synthetic data. In *2016 fourth international conference on 3D vision (3DV)*. IEEE, 460–469.

Szymon Rusinkiewicz and Marc Levoy. 2001. Efficient variants of the ICP algorithm. In *Proceedings third international conference on 3-D digital imaging and modeling*. IEEE, 145–152.

Shunsuke Saito, Lingyu Wei, Liwen Hu, Koki Nagano, and Hao Li. 2017. Photorealistic facial texture inference using deep neural networks. In *Proceedings of the IEEE Conference on Computer Vision and Pattern Recognition*. 5144–5153.

Steven M Seitz, Brian Curless, James Diebel, Daniel Scharstein, and Richard Szeliski. 2006. A comparison and evaluation of multi-view stereo reconstruction algorithms. In *2006 IEEE computer society conference on computer vision and pattern recognition (CVPR'06)*, Vol. 1. IEEE, 519–528.

Unity Technologies. 2020. The Heretic: Digital Human. <https://assetstore.unity.com/packages/essentials/tutorial-projects/the-heretic-digital-human-168620>

Justus Thies, Michael Zollhofer, Marc Stamminger, Christian Theobalt, and Matthias Nießner. 2016. Face2face: Real-time face capture and reenactment of rgb videos. In *Proceedings of the IEEE conference on computer vision and pattern recognition*. 2387–2395.

Anh Tuan Tran, Tal Hassner, Iacopo Masi, and Gérard Medioni. 2017. Regressing robust and discriminative 3D morphable models with a very deep neural network. In *Proceedings of the IEEE conference on computer vision and pattern recognition*. 5163–5172.

Shih-En Wei, Jason Saragih, Tomas Simon, Adam W. Harley, Stephen Lombardi, Michal Perdoch, Alexander Hypes, Dawei Wang, Hernan Badino, and Yaser Sheikh. 2019. VR Facial Animation via Multiview Image Translation. *38*, 4, Article 67 (jul 2019), 16 pages. <https://doi.org/10.1145/3306346.3323030>

Thibaut Weise, Sofien Bouaziz, Hao Li, and Mark Pauly. 2011. Realtime performance-based facial animation. *ACM transactions on graphics (TOG)* 30, 4 (2011), 1–10.

Cyrus A Wilson, Abhijeet Ghosh, Pieter Peers, Jen-Yuan Chiang, Jay Busch, and Paul Debevec. 2010. Temporal upsampling of performance geometry using photometric alignment. *ACM Transactions on Graphics (TOG)* 29, 2 (2010), 1–11.

Chenglei Wu, Derek Bradley, Markus Gross, and Thabo Beeler. 2016. An anatomically-constrained local deformation model for monocular face capture. *ACM transactions on graphics (TOG)* 35, 4 (2016), 1–12.

Shugo Yamaguchi, Shunsuke Saito, Koki Nagano, Yajie Zhao, Weikai Chen, Kyle Olszewski, Shigeo Morishima, and Hao Li. 2018. High-fidelity facial reflectance and geometry inference from an unconstrained image. *ACM Transactions on Graphics (TOG)* 37, 4 (2018), 1–14.

Jae Shin Yoon, Takaaki Shiratori, Shouo-I Yu, and Hyun Soo Park. 2019. Self-supervised adaptation of high-fidelity face models for monocular performance tracking. In *Proceedings of the IEEE/CVF Conference on Computer Vision and Pattern Recognition*. 4601–4609.

Longwen Zhang, Qixuan Zhang, Minye Wu, Jingyi Yu, and Lan Xu. 2021. Neural Video Portrait Relighting in Real-time via Consistency Modeling. *arXiv preprint arXiv:2104.00484* (2021).

Zhanpeng Zhang, Ping Luo, Chen Change Loy, and Xiaoou Tang. 2014. Facial landmark detection by deep multi-task learning. In *European conference on computer vision*. Springer, 94–108.

Michael Zollhöfer, Justus Thies, Pablo Garrido, Derek Bradley, Thabo Beeler, Patrick Pérez, Marc Stamminger, Matthias Nießner, and Christian Theobalt. 2018. State of the art on monocular 3D face reconstruction, tracking, and applications. In *Computer Graphics Forum*, Vol. 37. Wiley Online Library, 523–550.